nature cell biology

Control of plasma membrane lipid homeostasis by the extended synaptotagmins

Yasunori Saheki[1,2,3,4,5,8], Xin Bian[1,2,3,4,5,9], Curtis M. Schauder[2,9], Yujin Sawaki[1,2,3,4,5], Michal A. Surma[6], Christian Klose[6], Frederic Pincet[2,7], Karin M. Reinisch[2] and Pietro De Camilli[1,2,3,4,5,10]

Acute metabolic changes in plasma membrane (PM) lipids, such as those mediating signalling reactions, are rapidly compensated by homeostatic responses whose molecular basis is poorly understood. Here we show that the extended synaptotagmins (E-Syts), endoplasmic reticulum (ER) proteins that function as PtdIns(4,5)P_2- and Ca^{2+}-regulated tethers to the PM, participate in these responses. E-Syts transfer glycerolipids between bilayers *in vitro*, and this transfer requires Ca^{2+} and their lipid-harbouring SMP domain. Genome-edited cells lacking E-Syts do not exhibit abnormalities in the major glycerolipids at rest, but exhibit enhanced and sustained accumulation of PM diacylglycerol following PtdIns(4,5)P_2 hydrolysis by PLC activation, which can be rescued by expression of E-Syt1, but not by mutant E-Syt1 lacking the SMP domain. The formation of E-Syt-dependent ER–PM tethers in response to stimuli that cleave PtdIns(4,5)P_2 and elevate Ca^{2+} may help reverse accumulation of diacylglycerol in the PM by transferring it to the ER for metabolic recycling.

The endoplasmic reticulum (ER) carries out a multiplicity of functions, including protein and lipid synthesis, lipid metabolism and Ca^{2+} storage for intracellular signalling. Whereas membranes of the ER are functionally connected to all membranes of the secretory and endocytic pathways via vesicular transport, they fuse only with each other and with vesicles involved in retrograde transport to this organelle. However, close appositions between the ER and the membranes of all other membranous organelles, including the plasma membrane (PM), play major roles in cellular physiology. For example, ER membrane contact sites are involved in the control of Ca^{2+} homeostasis, in exchanges of lipids between bilayers, and in the function of ER-localized enzymes that act *in trans* on the apposed membrane[1–7].

One class of tethers that mediate ER–PM contacts are the three extended synaptotagmins (E-Syts) (tricalbins in yeast)[8–11]. E-Syts, which occur as homo and heterodimers, are embedded into the ER through an amino-terminal membrane anchor that is followed by an SMP (synaptotagmin-like, mitochondrial-lipid-binding protein) domain and multiple C2 domains (five in E-Syt1 and three in E-Syt2 and E-Syt3). Their tethering function is mediated by C2 domain-dependent interactions with the PtdIns(4,5)P_2 in the PM and are additionally regulated by cytosolic Ca^{2+} (refs 8,12). The E-Syts resemble classical synaptotagmin[13] in domain structure. However, whereas synaptotagmin is exported from the ER and tethers secretory vesicles to the PM in preparation for Ca^{2+}-dependent fusion, the E-Syts are retained in the ER. Interestingly, all proteins previously considered synaptotagmin homologues in plants contain SMP domains and are ER proteins[14–17].

SMP domains are members of a superfamily of modules, the TULIP domains, which are found in extra- and intracellular proteins and whose shared property is their ability to harbour lipids in a hydrophobic cavity[18–22]. One of the best-studied TULIP domain proteins is CETP, which mediates transport of lipids between high- and low-density lipoprotein[20]. SMP domains comprise modules that are localized intracellularly at membrane contact sites[9,23]. As revealed by crystallography, the SMP domain of E-Syt2 dimerizes to form a ~90-Å-long cylinder traversed by a deep groove lined with hydrophobic residues that contains lipids[22]. Supporting these findings, mass spectrometry of SMP domains detected the presence of glycerolipids[22,24].

The precise role of the E-Syts in cell physiology remains unclear. A plausible scenario is that they function in the delivery of newly

[1]Department of Neuroscience, Yale University School of Medicine, New Haven, Connecticut 06510, USA. [2]Department of Cell Biology, Yale University School of Medicine, New Haven, Connecticut 06510, USA. [3]Howard Hughes Medical Institute, Yale University School of Medicine, New Haven, Connecticut 06510, USA. [4]Kavli Institute for Neuroscience, Yale University School of Medicine, New Haven, Connecticut 06510, USA. [5]Program in Cellular Neuroscience, Neurodegeneration and Repair, Yale University School of Medicine, New Haven, Connecticut 06510, USA. [6]Lipotype GmbH, Am Tatzberg 47-49, 01307 Dresden, Germany. [7]Laboratoire de Physique Statistique, Ecole Normale Supérieure de Paris, Université Pierre et Marie Curie, Université Paris Diderot, Centre National de la Recherche Scientifique, UMR 8550, 24 rue Lhomond, 75005 Paris, France. [8]Present address: Lee Kong Chian School of Medicine, Nanyang Technological University, 308232, Singapore. [9]These authors contributed equally to this work.
[10]Correspondence should be addressed to P.D.C. (e-mail: pietro.decamilli@yale.edu)

Received 13 August 2015; accepted 11 March 2016; published online 11 April 2016; corrected online 14 April 2016; DOI: 10.1038/ncb3339

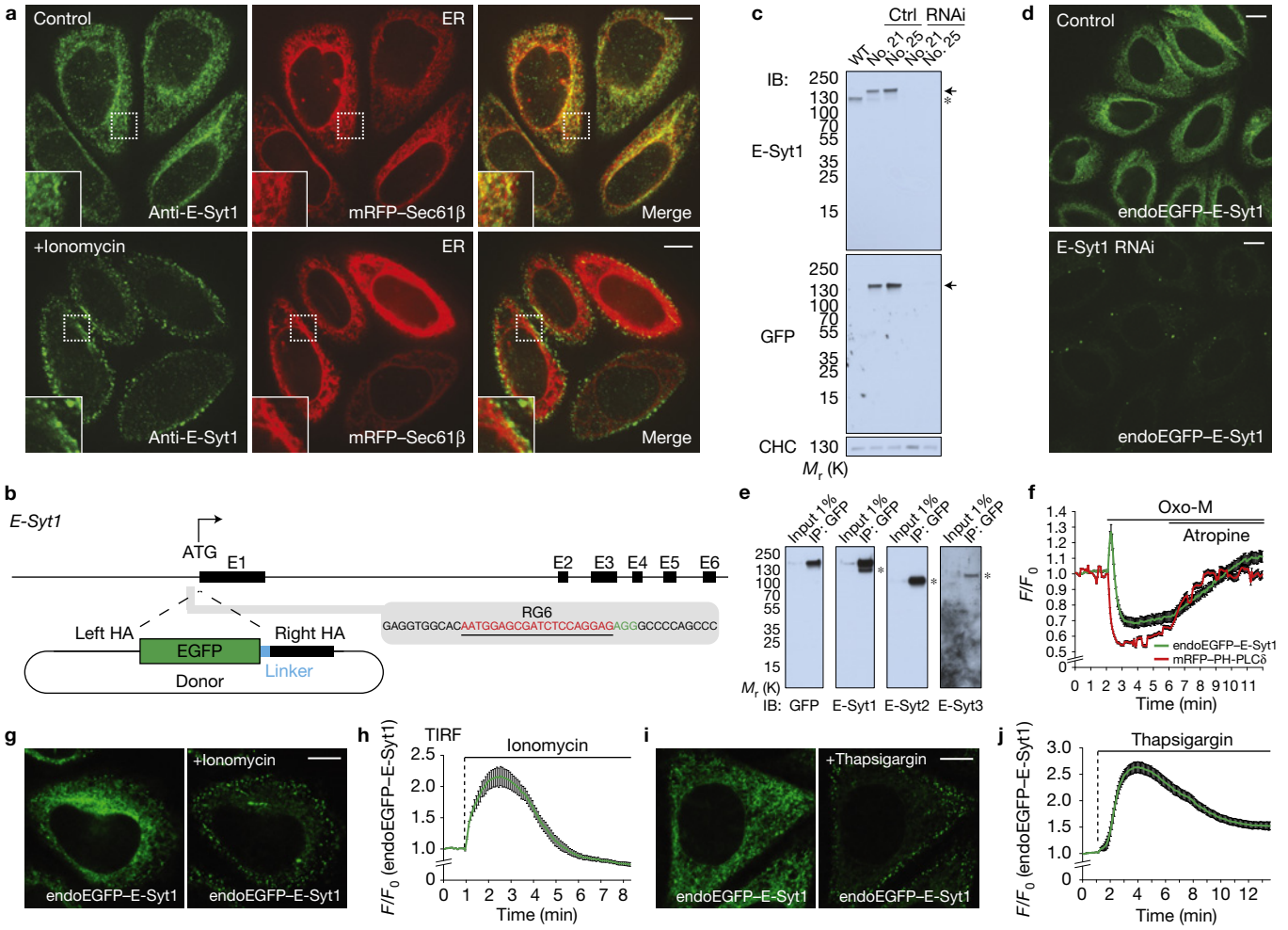

Figure 1 Localization of endogenous E-Syt1. (**a**) Confocal images of HeLa cells expressing mRFP–Sec61β. Localization of endogenous E-Syt1 was detected by an affinity-purified antibody. Insets show higher magnifications of the areas framed by dotted boxes. Bottom images: HeLa cells stimulated with ionomycin (2 μM) for 1 min. Note the translocation of the E-Syt1 fluorescent signals to the cortical region of the cell. (**b**) Strategy for the endogenous tagging of E-Syt1 (see Methods). (**c**) Lysates of control HeLa cells, two endogenously tagged HeLa cell lines (no. 21 and no. 25), and the same two lines treated with RNAi against endogenous E-Syt1 were processed by SDS–PAGE and immunoblotting (IB) with anti-E-Syt1, anti-GFP and anti-clathrin heavy chain (CHC) antibodies. Arrows and an asterisk indicate endogenously tagged EGFP–E-Syt1 and endogenous E-Syt1, respectively. (**d**) Confocal images of live no. 21 cells showing endogenously tagged EGFP–E-Syt1 (endoEGFP–E-Syt1) fluorescent signals in control but not in RNAi-treated cells. (**e**) Extracts of no. 21 cells were subjected to anti-GFP immunoprecipitation (IP) and then processed by SDS–PAGE and immunoblotting with the indicated antibodies. Asterisks indicate co-immunoprecipitated bands corresponding to endogenous untagged proteins. Note the strong homo- and heterodimerization of endogenously tagged E-Syt1 with endogenous E-Syt1, E-Syt2 and E-Syt3. (**f**) Time course of normalized GFP signal, as assessed by total internal reflection fluorescence (TIRF) microscopy, from cells expressing endogenously tagged E-Syt1 as well as muscarinic M1 receptor (M1R) and the PtdIns(4,5)P_2 probe, mRFP–PH-PLCδ. Oxo-M (10 μM) stimulation and atropine (50 μM) application are indicated. The biphasic response of E-Syt1 reflects the increase in cytosolic Ca^{2+} immediately followed by massive PtdIns(4,5)P_2 depletion (mean ± s.e.m., $n = 16$ cells pooled from two independent experiments). (**g–j**) Confocal images of live clone no. 21 cells before and 1.5 min after stimulation with ionomycin (2 μM; **g**), and before and 4 min after stimulation with thapsigargin (2 μM; **i**); the time course of ionomycin-induced (**h**) and thapsigargin-induced (**i**) recruitment of endoEGFP–E-Syt1 to the PM, as assessed by TIRF microscopy, is also shown (mean ± s.e.m., $n = 8$ cells (**h**) and 11 cells (**j**) assessed from one experiment that was repeated independently three times with similar results). Scale bars, 10 μm. Unprocessed original scans of blots are shown in Supplementary Fig. 7.

synthesized lipids from the ER to the PM and/or of lipid metabolites from the PM to the ER for metabolic recycling. As their tethering properties are regulated by Ca^{2+}, their functions may be important in maintaining or resetting lipid homeostasis in response to acute physiological changes that produce PM lipid perturbations.

The goal of this study was to directly test the lipid transfer properties of the E-Syts and to begin determining their impact on lipid homeostasis at the PM in living cells.

RESULTS

Endogenous E-Syt1 is rapidly translocated to ER–PM contacts on cytosolic Ca^{2+} increase

Previous E-Syt localization studies had capitalized on exogenously expressed tagged proteins. We have now generated polyclonal antibodies against the N terminus of human E-Syt1, which on affinity-purification labelled specifically the endogenous protein in HeLa cells not only by western blotting (Supplementary Fig. 1a)

but also by immunofluorescence (Fig. 1a). The signal generated by these antibodies co-localized with mRFP–Sec61β (a marker of the ER membrane) and was absent in genome-edited HeLa cells lacking E-Syt1 (see below; Supplementary Fig. 1b). The bulk of this immunoreactivity rapidly translocated to the cell cortex (peak of recruitment at about 2–3 min) after addition of the Ca^{2+} ionophore ionomycin[25] (Fig. 1a), confirming results obtained with exogenous tagged E-Syt1 (Supplementary Fig. 1c,d)[8].

To analyse the dynamics of E-Syt1 when expressed at endogenous levels, a HeLa cell line expressing tagged E-Syt1 from the endogenous locus was generated by inserting EGFP at its N terminus using CRISPR/Cas9-mediated genome editing (Fig. 1b). Expression of the fusion protein (endoEGFP–E-Syt1) was confirmed by western blotting, which revealed a band reactive for both anti-GFP and anti-E-Syt1 antibodies in extracts of these cells (Fig. 1c). This band, as well as EGFP fluorescence, disappeared on RNA interference (RNAi) against endogenous E-Syt1 (Fig. 1c,d). Further analysis demonstrated that this protein had the expected properties and dynamics[8] of E-Syt1. These included homodimerization as well as heterodimerization with other E-Syts (Fig. 1e) and Ca^{2+}-dependent PM recruitment. This recruitment was very transient in response to the Ca^{2+} elevation produced by muscarinic M1 receptor (M1R) activation by oxotremorine M (Oxo-M) in cells overexpressing M1R[26], as this elevation is the result of PLC-dependent inositol 1,4,5-trisphosphate generation[27,28] and thus correlates with very rapid and massive PtdIns(4,5)P_2 depletion (Fig. 1f). It was more persistent, as expected[8], in response to Ca^{2+} elevations produced by ionomycin (Fig. 1g,h and Supplementary Video 1), which induces a slower PtdIns(4,5)P_2 loss (see below) and to thapsigargin (Fig. 1i,j and Supplementary Video 2), which does not have a major impact on PtdIns(4,5)P_2 levels.

Ca^{2+}-regulated E-Syt1-dependent lipid transport *in vitro*

The presence of the SMP domain in the E-Syts suggested a role for these proteins in lipid transfer[22]. To provide direct evidence for such a function, we tested the ability of the cytosolic domain of E-Syt1 to transfer lipids between liposomes using a fluorescence resonance energy transfer(FRET)-based assay (Fig. 2a). In this assay, donor liposomes comprising phosphatidylcholine (PC), a fluorescent dye-labelled lipid (NBD–phosphatidylethanolamine (PE) (Fig. 2b)) and a nickel-conjugated lipid (DGS–NTA(Ni)), but no acidic phospholipids (and thus ER-like) were mixed with acceptor acidic phospholipid-containing (PM-like) liposomes (PC, phosphatidylserine (PS) and PtdIns(4,5)P_2) and with the purified His-tagged cytosolic portion of E-Syt1 (E-Syt1$_{cyto}$) (Fig. 2a). This construct becomes anchored to the donor liposomes by the His tag and binds PtdIns(4,5)P_2-containing acceptor liposomes *in trans*, and in a Ca^{2+}-dependent way, by means of its C2 domains (Fig. 2a).

In the absence of E-Syt1$_{cyto}$, NBD–PE was self-quenched in the donor liposomes, and solubilization of the liposomes with *n*-dodecyl-ß-D-maltoside resulted in an efficient dequenching (Supplementary Fig. 2a).

Addition of E-Syt1$_{cyto}$ and of various Ca^{2+} concentrations (5 to 200 μM) to the donor plus acceptor liposome mixture induced rapid dequenching of NBD–PE in a Ca^{2+}-dependent manner, consistent with the transfer of NBD–PE from donor to acceptor liposomes (Fig. 2c,d). Fluorescent lipids (1%) and 100 μM Ca^{2+} were used in subsequent transfer assays. Absence of PtdIns(4,5)P_2 in the acceptor liposomes markedly slowed the dequenching of NBD–PE (Supplementary Fig. 2b). Furthermore, lipid transfer was bidirectional, as incorporating NBD–PE in either the ER-like or the PM-like liposomes, that is, reverting donor and acceptor liposomes, resulting in dye dequenching with the same efficiency (Supplementary Fig. 2c). NBD–PE dequenching was not due to membrane fusion as a similar assay in which the fluorescent lipid tag in the donor liposomes was replaced by a water-soluble luminal self-quenching dye (sulforhodamine B) revealed no content mixing of the liposomes (Supplementary Fig. 2d). Potential lipid mixing due to hemifusion as a result of liposome tethering was ruled out: as revealed by turbidity assay, the potent liposome tethering produced by E-Syt1$_{cyto}$ could be completely reversed by the addition of a cocktail of EDTA, imidazole and proteinase K ('Cocktail'; (Fig. 2e,h top panels). Furthermore, a mutant E-Syt1$_{cyto}$ lacking the SMP domain (E-Syt1$_{cyto}$ ΔSMP) had negligible lipid transfer activity, although its liposome tethering properties were only slightly reduced relative to E-Syt1$_{cyto}$ (Fig. 2e). This minor reduction could have been explained by the lack of SMP-dependent dimerization (Fig. 2e). Finally, replacing two hydrophobic residues (Val169 and Leu308) lining the lipid-binding groove of the SMP domain[22] with the bulky hydrophobic amino acid tryptophan strongly impaired lipid (NBD–PE) binding and transfer activity (Fig. 2f,g) without affecting liposome tethering (Fig. 2h).

Changing the ratio of donor and acceptor liposomes, from 1:9 to 1:1, significantly reduced the maximum dequenching efficiency achieved at the end of the assay (Supplementary Fig. 2e), indicating that E-Syt1 transfer glycerolipids along a concentration gradient. Furthermore, addition of non-labelled PE to acceptor liposomes did not affect NBD–PE transfer (Supplementary Fig. 2f), as PE is not preferred over other glycerolipids present in the liposome mixture (all glycerolipids are transported bidirectionally).

Having validated the hypothesis that an E-Syt has lipid transfer activity, we explored the role of the E-Syts in lipid dynamics and homeostasis with a gene knockout (KO) approach.

Generation of E-Syt1/2 DKO and E-Syt1/2/3 TKO HeLa cells using TALEN and CRISPR

We first disrupted the E-Syt2 gene in HeLa cells using transcription activator-like effector nuclease (TALEN) and then sequentially the E-Syt1 and the E-Syt3 genes in these cells using the CRISPR/Cas9 system (Fig. 3a and Supplementary Fig. 3a–c and see Methods for details).

Absence of the E-Syt1 and E-Syt2 bands in western blots of extracts of two E-Syt1/2 double-KO clones (DKO:6-8 and DKO:7-5) is shown in Fig. 3b, and the loss of E-Syt1 immunofluorescence in the DKO:6-8 clone is shown in Supplementary Fig. 1b (see also Supplementary Fig. 3d–g). Given the low expression level of endogenous E-Syt3, validation of its absence in triple-KO (TKO) cells required an enrichment procedure. To this end, we expressed EGFP-tagged E-Syt2 as a bait for E-Syt3 with which it heterodimerizes: anti-GFP immunoprecipitates obtained from these cells were enriched in the E-Syt3 immunoreactive band only when generated from cells where the E-Syt3 gene had not been edited, irrespective of the expression of the other endogenous E-Syts (Fig. 3b, see also Supplementary Fig. 3h), confirming successful KO of E-Syt3.

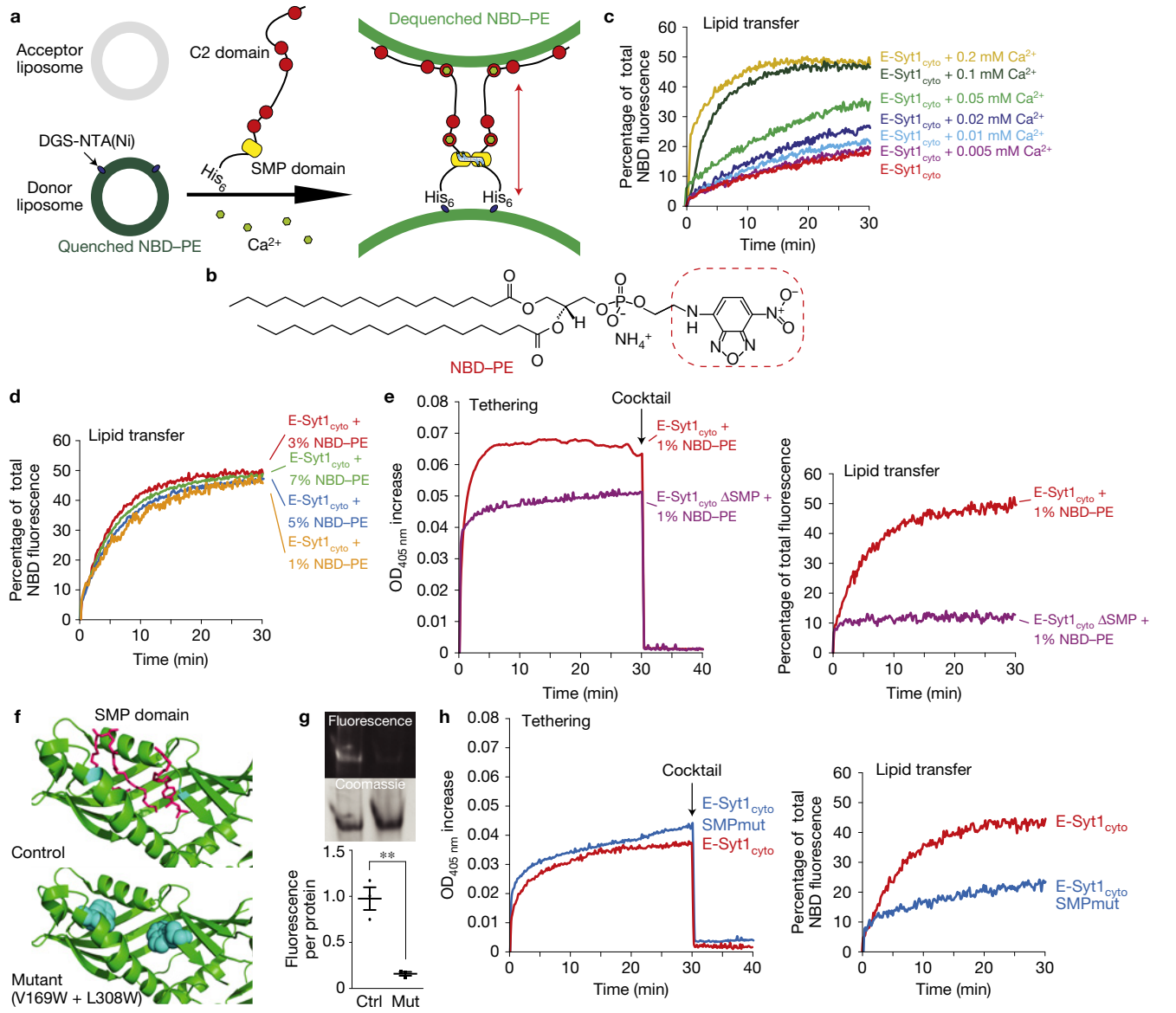

Figure 2 E-Syt1 is a Ca^{2+}-dependent lipid transfer protein. (**a**) Schematics showing the *in vitro* lipid transfer assay. Donor liposomes (PC, DGS-NTA(Ni), NBD–PE) and acceptor liposomes (PC, PS, PtdIns(4,5)P_2) were incubated with the histidine (His)-tagged cytosolic portion of the E-Syt1 protein (E-Syt1$_{cyto}$). Dequenching of self-quenched NBD–PE fluorescence, that is, transfer of the fluorescent lipids from donor to acceptor liposomes, was monitored using a fluorometer (see Methods). (**b**) Structure of NBD–PE. (**c**) Time course of normalized fluorescence signals from liposome mixtures containing 1% NBD–PE in the donor liposomes at the indicated concentration of Ca^{2+} in the assay buffer. E-Syt1$_{cyto}$ was added at time 0. (**d**) Time course of normalized fluorescence signals from E-Syt1$_{cyto}$/liposome mixtures containing different mole percents of NBD–PE in the donor liposomes and incubated with 100 μM Ca^{2+}. (**e**) Left: time course of turbidity of the suspension (see Methods). Turbidity reflects liposome clustering due to tethering of donor and acceptor liposomes. Right: time course of normalized fluorescence signals from liposome mixtures containing 1% NBD–PE in the donor liposomes and either E-Syt1$_{cyto}$ or E-Syt1$_{cyto}$ lacking the SMP domain (E-Syt1$_{cyto}$ ΔSMP). (**f**) Design of the mutant SMP domain defective in lipid harbouring. Hydrophobic amino acids lining the deep hydrophobic groove[22] were mutated to tryptophan, thus creating steric hindrance to access of acyl chains to the SMP channel. Aromatic rings of tryptophan are shown as surface representation. (**g**) Lipid binding of the E-Syt1 SMP domain. Top: purified WT SMP domain (Ctrl) and mutant SMP domain, carrying V169W and L308W mutations (Mut), were incubated with NBD–PE, run on native-PAGE and analysed by fluorometry and Coomassie blue staining. Bottom: quantification of fluorescence signals of NBD–PE normalized to the total amount of protein (mean ± s.e.m., $n=3$ independent experiments; two-tailed Student's t-test with equal variance, $P=0.0028$). (**h**) Left: time course of turbidity of the suspension. Right: time course of normalized fluorescence signals from liposome mixtures containing 1% NBD–PE in the donor liposomes and either E-Syt1$_{cyto}$ or E-Syt1$_{cyto}$ with lipid-binding-deficient SMP domain (E-Syt1$_{cyto}$ SMPmut). The transfer of NBD–PE is much reduced with E-Syt1$_{cyto}$ SMPmut. For all of the liposome-based assays, data are from one experiment; three experiments that yielded similar results were performed.

No obvious defects were observed in cell viability and overall morphology of KO cells, with the exception of a slower growth relative to parental HeLa cells. However, more detailed analysis revealed some changes, as described below. Initial experiments were carried out in E-Syt1/2 DKO cells. Subsequently, selected experiments were repeated in E-Syt TKO cells with similar

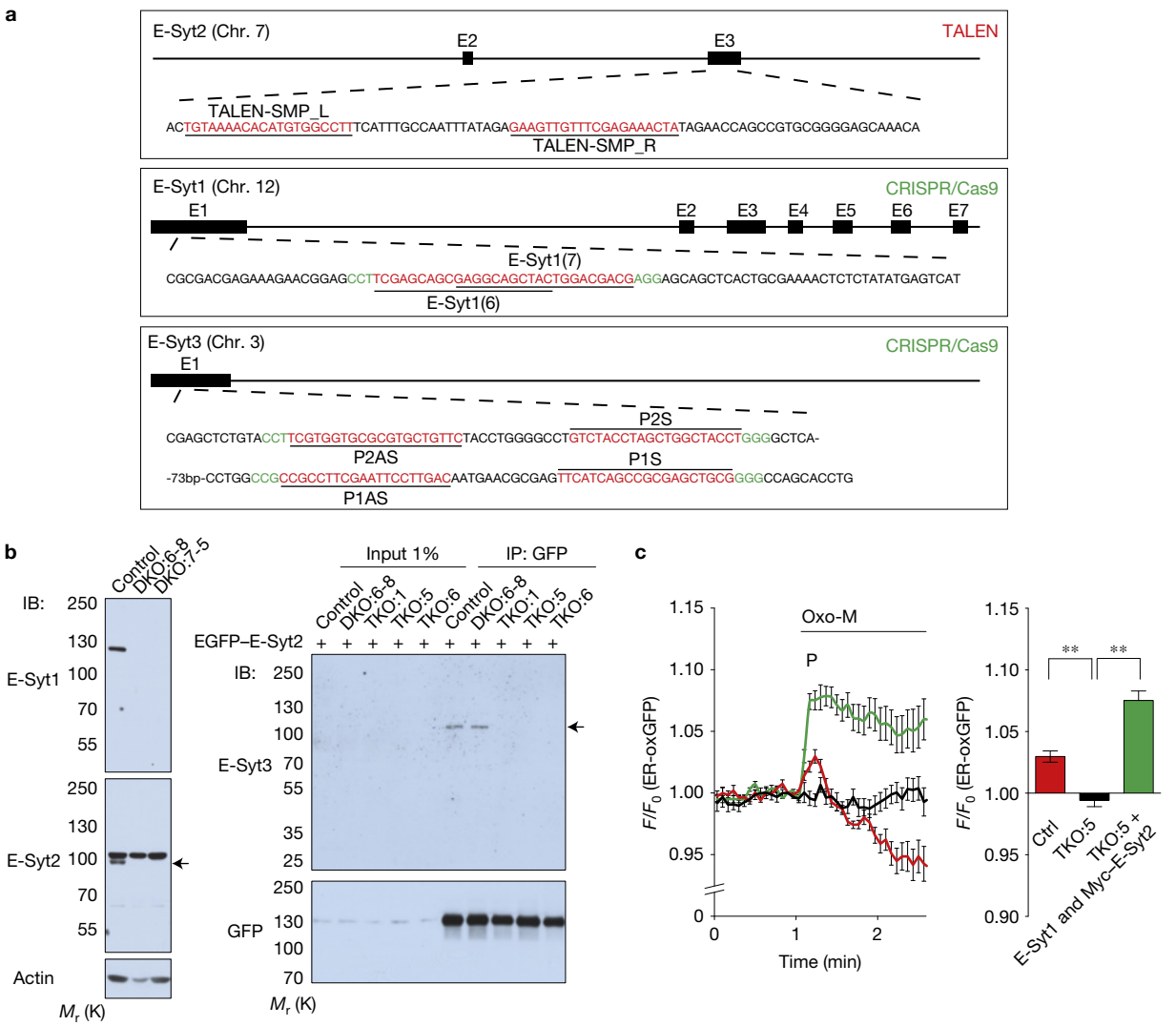

Figure 3 Generation of E-Syt1/2 DKO and E-Syt1/2/3 TKO HeLa cells using TALEN and CRISPR. (**a**) Schematics of the TALEN- and Cas9/sgRNA-targeting sites in human E-Syt2, E-Syt1 and E-Syt3 loci. The targeting sequence is underlined and highlighted in red. The protospacer-adjacent motif is labelled in green for E-Syt1 and E-Syt3 loci. (**b**) Left: lysates of control HeLa cells and two independently isolated E-Syt1/2 DKO cell lines were processed by SDS–PAGE and immunoblotting (IB) with anti-E-Syt1, anti-E-Syt2 and anti-actin antibodies. The arrow indicates the specific band for E-Syt2. Right: extracts of control HeLa cells, clone DKO:6-8 and three clones of E-Syt TKO cells transfected with EGFP–E-Syt2 were subjected to anti-GFP immunoprecipitation (IP) and then processed by SDS–PAGE and immunoblotting with anti-E-Syt3 and anti-GFP antibodies. The arrow indicates co-immunoprecipitated bands. Note the absence of IP-enriched E-Syt3 expression in E-Syt TKO cells. (**c**) Left: time course of normalized GFP signal, as assessed by TIRF microscopy, from WT control (Ctrl) and E-Syt TKO cells expressing a luminal ER marker (ER-oxGFP) and M1R. Oxo-M (10 μM) stimulation is indicated. Re-expression of E-Syt1 together with Myc-tagged E-Syt2 (Myc–E-Syt2) in TKO cells rescued the loss of ER dynamics. Right: quantification of fluorescence corresponding to the peak (indicated by 'P') for each quantification shown on the left (for both left and right panels, mean ± s.e.m., $n=7$ cells (Ctrl); $n=18$ cells (TKO:5); $n=18$ cells (TKO:5 + E-Syt1 and Myc–E-Syt2; data are pooled from three independent experiments except for Ctrl, which is from one experiment—the experiment was repeated independently two times with similar results); two-tailed Student's *t*-test with equal variance, Ctrl: $^{**}P=0.0028$, TKO:5 + E-Syt1 and Myc–E-Syt2: $^{**}P<0.0001$). Unprocessed original scans of blots are shown in Supplementary Fig. 7.

results, most likely because of the only low expression level of E-Syt3 (ref. 8).

Ca^{2+} enhanced apposition of the ER to the PM is impaired in E-Syt KO cells

As a premise to study the impact of the E-Syts on lipid dynamics, we assessed whether absence of the E-Syts had an impact on the ER in response to a rise in cytosolic Ca^{2+}. As reported, in wild-type (WT) cells, elevation of cytosolic Ca^{2+} results in increased fluorescence for the luminal ER marker (ER-oxGFP) in total internal reflection fluorescence (TIRF) microscopy, most likely reflecting an expansion of areas of apposition between the ER and the PM[8]. To assess the impact of the lack of the E-Syts on such a response, changes of the ER-oxGFP fluorescence following muscarinic receptor stimulation by Oxo-M were monitored in control and TKO cells also transfected with the muscarinic M1 receptor (M1R). In E-Syt

TKO cells, the Ca^{2+}-dependent increase of ER-oxGFP fluorescence (which is very transient owing to concomitant PtdIns(4,5)P_2 loss) was abolished and this effect could be 'rescued', in fact resulting in exaggeration of recruitment, by exogenous expression of E-Syt1 along with Myc–E-Syt2 (Fig. 3c) (note that the E-Syt1/E-Syt2 heterodimer is predominantly localized throughout the ER at resting Ca^{2+} levels, in contrast to the E-Syt2 homodimer that is already concentrated at the ER–PM contact sites at resting Ca^{2+} levels[8]). Near absence of the E-Syts does not inhibit store-operated calcium entry[8,12], thus ruling out impaired Ca^{2+} elevations as the cause of the defective increase of ER-oxGFP fluorescence.

The steady-state glycerolipid composition of the PM is not affected in E-Syt KO cells

The SMP domain of the E-Syts harbours glycerophospholipids[22] and can transfer them *in vitro* between artificial membranes (see above). As the E-Syts form ER–PM tethers, they may exchange such lipids between these two membranes.

To assess the impact of E-Syts in the control of steady-state PM lipid levels, we applied with some modifications a method for the rapid separation and purification of PMs from cultured cells[29]. HeLa cells in suspension were mixed with poly-D-lysine-coated dextran beads and the mixture was incubated overnight to allow the cells to adhere to the beads (Fig. 4a,c,d). The beads were then exposed to a hypotonic solution to induce osmotic lysis, vigorously vortexed and briefly sonicated to remove most organelles from the PM sheets that remained tightly attached to the bead surface and could be visualized by NBD-labelled sphingomyelin (Fig. 4b,e, and see Methods). As shown by western blotting, the material that remained bound to the beads was very strongly enriched relative to the starting material in PM marker proteins (CD44 and Na^+/K^+-ATPase). Other proteins tested partitioned roughly as expected. PM receptors (epidermal growth factor receptor (EGFR) and transferrin receptor (TfR)) were also present but not equally enriched in the PM fraction, in agreement with the presence of large pools of these receptors on endosomal membranes. The endosomal marker protein (EEA1) was greatly depleted, and the Golgi marker protein GM130 was absent, whereas small amounts of ER proteins recovered in the PM, such as calreticulin, VAPA, VAPB and STIM1, most likely reflect tightly attached cortical ER (Fig. 4f,g). Importantly, the recovery of endogenous E-Syt1 and E-Syt2 on bead-attached PM sheets was similar to that of other integral ER proteins (calreticulin, VAP and STIM1; Fig. 4g), further supporting their localization in the ER[8]. The similar subcellular recovery of endogenous E-Syt1 and E-Syt2 in the bead-bound material confirms that these two proteins are primarily present in cells as heterodimers localized throughout the ER, with only a small fraction of the heterodimer being already at ER–PM contact sites in control conditions[8].

Analysis by mass spectrometry of the major glycerolipid species in the PM fractions of WT and E-Syt KO cells did not reveal specific changes compared to total cellular lipids (individual extracts from DKO and TKO cells were independently analysed and then pooled as they had similar properties in all functional assays consistent with the very low abundance of E-Syt3 in HeLa cells[8]; Fig. 4h), thus speaking against a major role of the E-Syts in controlling the steady-state distribution of these lipids in the PM.

Sustained accumulation of diacylglycerol at the PM following activation of PLC in E-Syt KO cells

The E-Syts may play a role in homeostatic responses to conditions that acutely affect the lipid compositions of the PM. Transient increase in E-Syt1-dependent ER–PM tethers in response to activation of PLC-coupled receptors may be part of a mechanism to counteract PtdIns(4,5)P_2 loss in response to its hydrolysis. However, TIRF microscopy analysis of the PtdIns(4,5)P_2 probe mRFP–PH-PLCδ to monitor PtdIns(4,5)P_2 depletion and resynthesis at the PM in response to Oxo-M-induced PLC activation of overexpressed M1R did not reveal obvious defects in the absence of the E-Syts at any time point (Supplementary Fig. 4a). These findings speak against a major role of these proteins in the regulation of PtdIns(4,5)P_2 dynamics.

Another potential function of E-Syts in response to PLC activation is the control of the dynamics of diacylglycerol (DAG) generated by PtdIns(4,5)P_2 cleavage. Levels of PM DAG are very low at rest (Fig. 4h), transiently increase on PLC activation and then gradually return to normal levels[26]. TIRF microscopy of the fluorescence signal of C1–mCherry (mCherry–C1 domains of PKCδ)[30], a DAG probe, showed that the increase of this lipid in the PM on stimulation of endogenous PLC-coupled histamine receptor was more sustained in the absence of the E-Syts. Importantly, the expression of EGFP–E-Syt1 together with Myc–E-Syt2 rescued the phenotype (Fig. 5a). Although the increase of DAG occurs at the expense of PtdIns(4,5)P_2 cleavage, under these conditions (endogenous histamine receptor levels) only modest PtdIns(4,5)P_2 hydrolysis was observed (Supplementary Fig. 4b). Thus, a basal pool of E-Syts could still bind to the PM (Supplementary Fig. 4b) in contrast to what happens on Oxo-M stimulation of M1R-overexpressing cells, when PtdIns(4,5)P_2 was rapidly depleted (Supplementary Fig. 4c), leading to rapid and massive dissociation of the E-Syts from the PM.

We also tested the effect of ionomycin, whose stimulation of Ca^{2+} influx also results in massive, but somewhat delayed, PLC-dependent hydrolysis of PtdIns(4,5)P_2 (ref. 31) so that E-Syt1 is recruited at the PM before complete PtdIns(4,5)P_2 depletion (see Fig. 5b for the recruitment of endogenously tagged E-Syt1, endoEGFP–E-Syt1). A very robust recruitment of C1–mCherry to the PM of these cells was observed in response to ionomycin (Fig. 5b,c), as detected by TIRF microscopy. Even with this drug, the accumulation of DAG (C1–mCherry fluorescence) in cells lacking E-Syts was more sustained in time relative to WT cells. Re-expression of either EGFP–E-Syt1 together with Myc–E-Syt2 (Fig. 5c,d) or EGFP–E-Syt1 alone (Fig. 5e) rescued the phenotype, but a mutant EGFP–E-Syt1 lacking the SMP domain did not (Fig. 5e), supporting a role for E-Syt1 in the regulation of DAG dynamics through an SMP-dependent mechanism. Prolonged accumulation of DAG on activation of PLC in E-Syt KO cells was further confirmed by another DAG probe, YFP–DBD (YFP fused to the C1b domain of PKCβII)[32] (Supplementary Fig. 5a).

Ca^{2+}-dependent DAG transfer by E-Syt1 *in vitro*

The cell-free assay shown in Fig. 2 demonstrates that E-Syt1 can transfer a glycerolipid, and thus, most likely also DAG. However, the ability of E-Syt1 to mediate Ca^{2+}-stimulated DAG transfer was directly assessed. As DAG does not have a headgroup that can be labelled with NBD, a radioactivity-based *in vitro* assay was used. 'Heavy' (sucrose loaded) liposomes composed of PC,

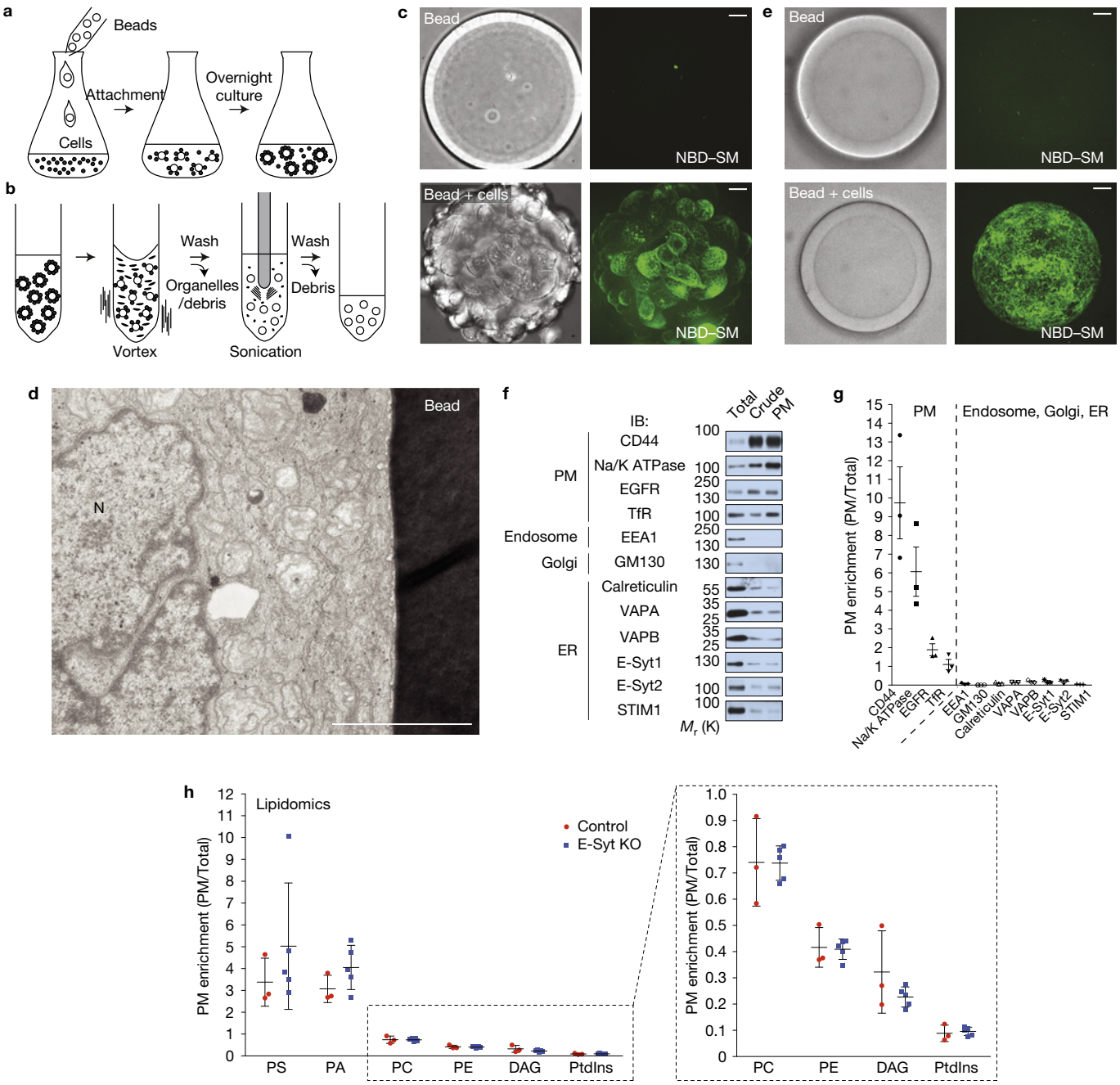

Figure 4 Rapid isolation and characterization of PM sheets. (**a**) Schematics showing the attachment of HeLa cells to dextran beads. Cells were dissociated and dextran beads were added drop by drop; the cell–bead mixture was then incubated with gentle stirring to allow uniform attachment and further incubated overnight. (**b**) Schematics showing the isolation of bead-attached PMs. Following a wash, the cell–bead mixture was exposed to a hypotonic buffer and vortexed to lyse cells and remove intracellular organelles. After extensive washes, a sonication pulse was applied to the beads to further remove intracellular organelles/debris from bead-attached PMs. (**c**) Confocal image of live HeLa cells attached to a bead. Top: bead without cells. Bottom: bead coated with HeLa cells as illustrated in **a**. Maximum projections of the serial *Z*-stack of confocal images are shown. The bead-attached PMs were stained with NBD-labelled sphingomyelin (NBD–SM, green). Scale bars, 20 μm. (**d**) Electron micrograph of a HeLa cell attached to a bead. N, nucleus. Scale bar, 5 μm. (**e**) Confocal images of beads after sonication and staining with NBD–SM. Top: bead not incubated with cells. Bottom: bead with PM sheets. Scale bars, 20 μm. (**f**) Bead-attached material (total lysate (Total), crude PM sheets before sonication (Crude) and final PM sheets (PM)) was processed by SDS–PAGE and immunoblotting (IB) with the indicated antibodies. Note the enrichment of PM proteins and depletion of ER, endosomal and Golgi proteins in the PM fractions. (**g**) Quantification of protein abundance as analysed in **f**. PM enrichment plots the ratio of 'PM' over 'Total' protein abundance (mean ± s.e.m., $n=3$ extracts). (**h**) Comparisons of PM glycerolipid profiles of WT (Control) and E-Syt KO HeLa cells (pooled values of DKO and TKO cells) as analysed by mass spectrometry. PM enrichment plots the ratio of PM lipids over total lipids (see Methods) (mean ± s.d., $n=3$ extracts (Control), $n=5$ extracts (three biologically independent samples from DKO:6-8 and two biologically independent samples from TKO:5 were pooled as DKO and TKO cells had similar properties in all functional assays consistent with the very low abundance of E-Syt3 in HeLa cells)). PS, phosphatidylserine; PA, phosphatidic acid; PC, phosphatidylcholine; PE, phosphatidylethanolamine; DAG, diacylglycerol; PtdIns, phosphatidylinositol. Unprocessed original scans of blots are shown in Supplementary Fig. 7.

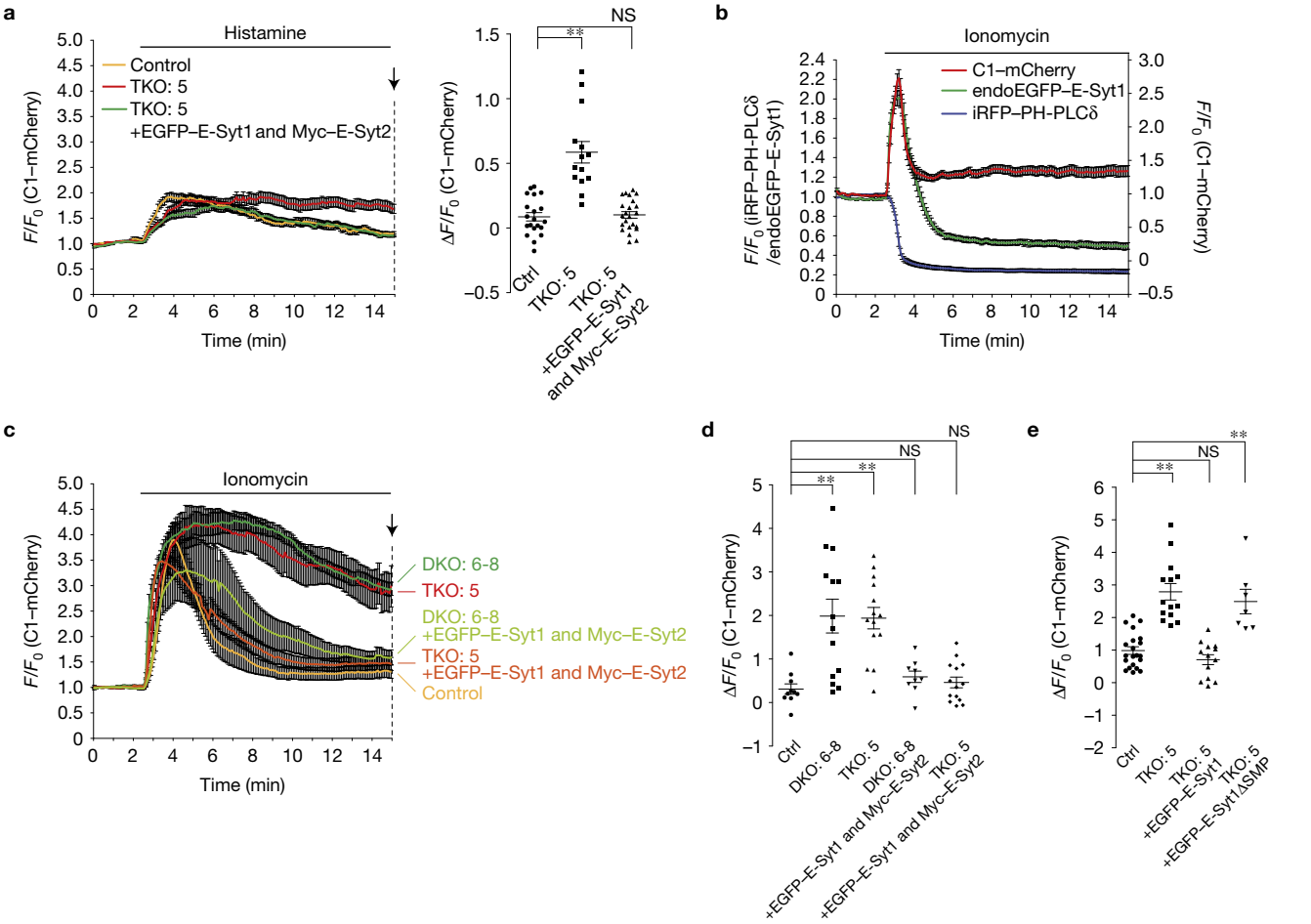

Figure 5 Prolonged accumulation of DAG in E-Syt KO cells on phospholipase activation. (**a**) Time course of normalized mCherry signal, as assessed by TIRF microscopy, from WT control (Ctrl) and E-Syt TKO cells expressing a DAG probe (C1–mCherry). Histamine (1 mM) stimulation is indicated. Re-expression of EGFP-tagged E-Syt1 (EGFP–E-Syt1) together with Myc–E-Syt2 in E-Syt TKO cells rescued the accumulation of DAG, as monitored by C1–mCherry. Right: values of $\Delta F/F_0$ corresponding to the end of the experiment as indicated by an arrow (mean ± s.e.m., $n=20$ cells (Ctrl), $n=14$ cells (TKO:5), $n=23$ cells (TKO:5 + EGFP–E-Syt1 and Myc–E-Syt2); data are pooled from two independent experiments except for Ctrl, which is pooled from three independent experiments; Bonferroni's multiple comparisons test, $^{**}P=0.0005$). (**b**) Time course of normalized EGFP, iRFP (left axis) and mCherry (right axis) signal, as assessed by TIRF microscopy, from cells expressing E-Syt1 tagged with EGFP at the endogenous locus (endoEGFP–E-Syt1) as well as a PtdIns(4,5)P_2 probe (iRFP–PH-PLCδ) and a DAG probe (C1–mCherry). Ionomycin (2 μM) stimulation is indicated (mean ± s.e.m., $n=6$ cells assessed from one experiment; the experiment was repeated independently three times, with similar results). (**c**) Time course of normalized mCherry signal, as assessed by TIRF microscopy, from WT control (Ctrl), E-Syt1/2 DKO cells and E-Syt TKO cells expressing C1–mCherry. Ionomycin (2 μM) stimulation is indicated. Re-expression of EGFP–E-Syt1 together with Myc–E-Syt2 in E-Syt1/2 DKO and E-Syt TKO cells rescued the accumulation of DAG, as monitored by C1–mCherry. (**d**) Values of $\Delta F/F_0$ corresponding to the end of the experiment as indicated by the arrow in **c** (mean ± s.e.m., $n=10$ cells (Ctrl), $n=14$ cells (DKO:6-8), $n=14$ cells (TKO:5), $n=9$ cells (DKO:6-8 + EGFP–E-Syt1 and Myc–E-Syt2), $n=14$ cells (TKO:5 + EGFP–E-Syt1 and Myc–E-Syt2); data are pooled from two independent experiments for each condition; Bonferroni's multiple comparisons test $P=0.0001$ (DKO:6-8); $P=0.0002$ (TKO:5)). (**e**) Values of $\Delta F/F_0$ corresponding to the end of the experiment as assayed in the same way as in **c** (mean ± s.e.m., $n=21$ cells (Ctrl), $n=14$ cells (TKO:5), $n=13$ cells (TKO:5 + EGFP–E-Syt1), $n=7$ cells (TKO:5 + EGFP–E-Syt1ΔSMP); data are pooled from two independent experiments except for TKO:5 + EGFP–E-Syt1ΔSMP, which is assessed from one experiment—the experiment was repeated independently two times, with similar results; Bonferroni's multiple comparisons test, $^{**}P<0.0001$). NS, not significant (cutoff $P>0.05$).

PS, PtdIns(4,5)P_2 and supplemented with ^{3}H-DAG were mixed in the presence or absence of 100 μM Ca^{2+} with 'light' (no sucrose) liposomes composed of PC and DGS-NTA(Ni) and with either the purified His-tagged E-Syt1$_{cyto}$ or E-Syt1$_{cyto}$ lacking the SMP domain (E-Syt1$_{cyto}$ΔSMP) (Fig. 6a, and see Methods). Subsequently, E-Syt1-tethered donor and acceptor liposomes were separated by the addition of a cocktail of imidazole and proteinase K followed by centrifugation (Fig. 6b). Analysis of radioactivity in the two populations of liposomes revealed robust SMP-domain-dependent and Ca^{2+}-stimulated ^{3}H-DAG accumulation in light liposomes, proving the ability of E-Syt1 to transport DAG (Fig. 6c).

Ca^{2+}-dependent recruitment of E-Syt1 in KO cells extracts DAG from the PM

A mechanism accounting for the clearance of excess DAG from the PM is its conversion to PA by DAG kinases (DGK)[33]. The lipid transport protein Nir2 is recruited to ER–PM contacts in a DAG- and phosphatidic acid (PA)-dependent manner following PLC-dependent

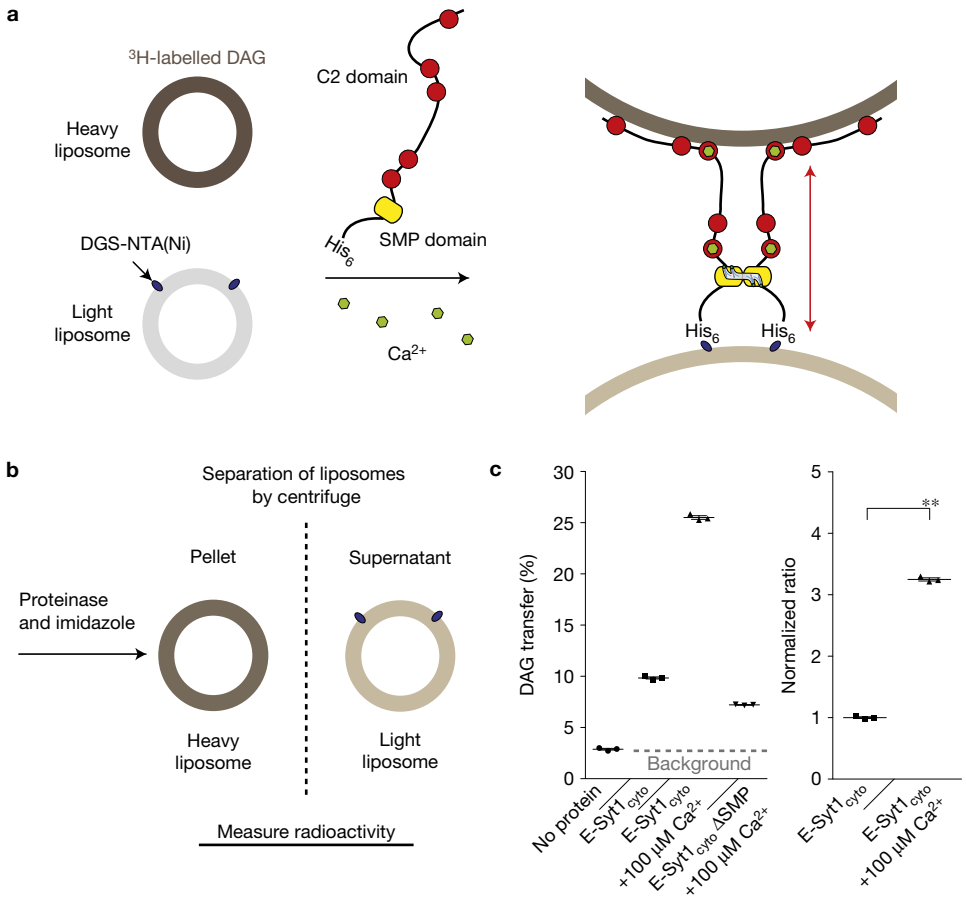

Figure 6 SMP-domain-dependent and Ca^{2+}-regulated diacylglycerol transfer by E-Syt1. (**a**) Schematics of the ^{3}H-DAG *in vitro* transfer assay. (**b**) A mixture of 'heavy' donor liposomes containing ^{3}H-DAG and 'light' acceptor liposomes was incubated for 10 min in the presence of 100 µM Ca^{2+} and either E-Syt1$_{cyto}$ or E-Syt1$_{cyto}$ lacking the SMP domain (E-Syt1$_{cyto}$ΔSMP). Next, the two populations of liposomes were separated by addition of proteinase K and imidazole followed by centrifugation. (**c**) Quantification of DAG transfer. Left: values are plotted as the percentage of ^{3}H radioactivity in the supernatant (that is, light acceptor liposomes) over the sum of the total radioactivity in the supernatant and pellet (that is, light and heavy donor liposomes). Right: normalized Ca^{2+}-dependence of E-Syt1-mediated DAG transfer was plotted after background subtraction (mean ± s.e.m., $n=3$ independent experiments for all of the conditions; two-tailed Student's *t*-test with equal variance, $^{**}P<0.0001$).

PtdIns(4,5)P_2 hydrolysis and transfers PA to the ER for metabolic recycling[34,35] (Fig. 7a). E-Syt- and Nir2-dependent mechanisms may cooperate in the recycling of these PtdIns(4,5)P_2 metabolites.

To assess the interplay of E-Syts with Nir2 in the clearance of DAG, we inhibited its conversion to PA using the DGK inhibitor DGKi during the recovery phase from an Oxo-M-dependent stimulus in M1R-expressing cells. As assessed by TIRF microscopy, Oxo-M-triggered PLC activity resulted in a rapid rise of DAG, which was reversed by the M1R antagonist atropine (Fig. 7b). The rate of DAG removal during atropine treatment, that is, when Ca^{2+} levels have returned to normal[27], was not substantially affected by the absence of the E-Syts (Supplementary Fig. 6a). Addition of DGKi together with atropine, blocked the gradual DAG loss, as expected (Fig. 7c). However, addition of ionomycin 2.5 min following atropine/DGKi application to HeLa cells expressing E-Syt1 EGFP-tagged at the endogenous locus triggered robust recruitment of endoEGFP–E-Syt1 to the PM and rapid loss of the DAG reporter C1–mCherry (Fig. 7d). Both DAG removal and E-Syt1 recruitment required the presence of extracellular Ca^{2+} (Supplementary Fig. 6b). Importantly, in cells lacking E-Syts (TKO cells), ionomycin did not produce a loss of DAG signal in the PM and re-expression of EGFP–E-Syt1 alone, but not of E-Syt1 lacking the SMP domain (Fig. 7e,f) or its ER anchor[8] (Supplementary Fig. 6c), was sufficient to rescue the phenotype. Mutations of the hydrophobic pockets of the SMP domain (see above) also significantly reduced rescuing activity (Fig. 7e,f).

These results support a role for E-Syt1 in exchanging lipids between the PM and the ER and the presence of a pathway that acts in parallel to Nir2 for the clearance of PtdIns(4,5)P_2 metabolites (Fig. 7a). However, further analyses suggested that the PM recruitments of Nir2 and of E-Syt1 can be decoupled. Simultaneous imaging of Nir2–mCherry and endoEGFP–E-Syt1 showed that Nir2 is rapidly recruited to the PM on triggered massive Oxo-M-triggered PLC-dependent PtdIns(4,5)P_2 cleavage as reported previously[34,36,37] (Fig. 7g). This rise occurred even when the E-Syts dissociated from the PM owing to PtdIns(4,5)P_2 depletion after a very transient Ca^{2+}-dependent recruitment before the drop of PtdIns(4,5)P_2. Conversely, during

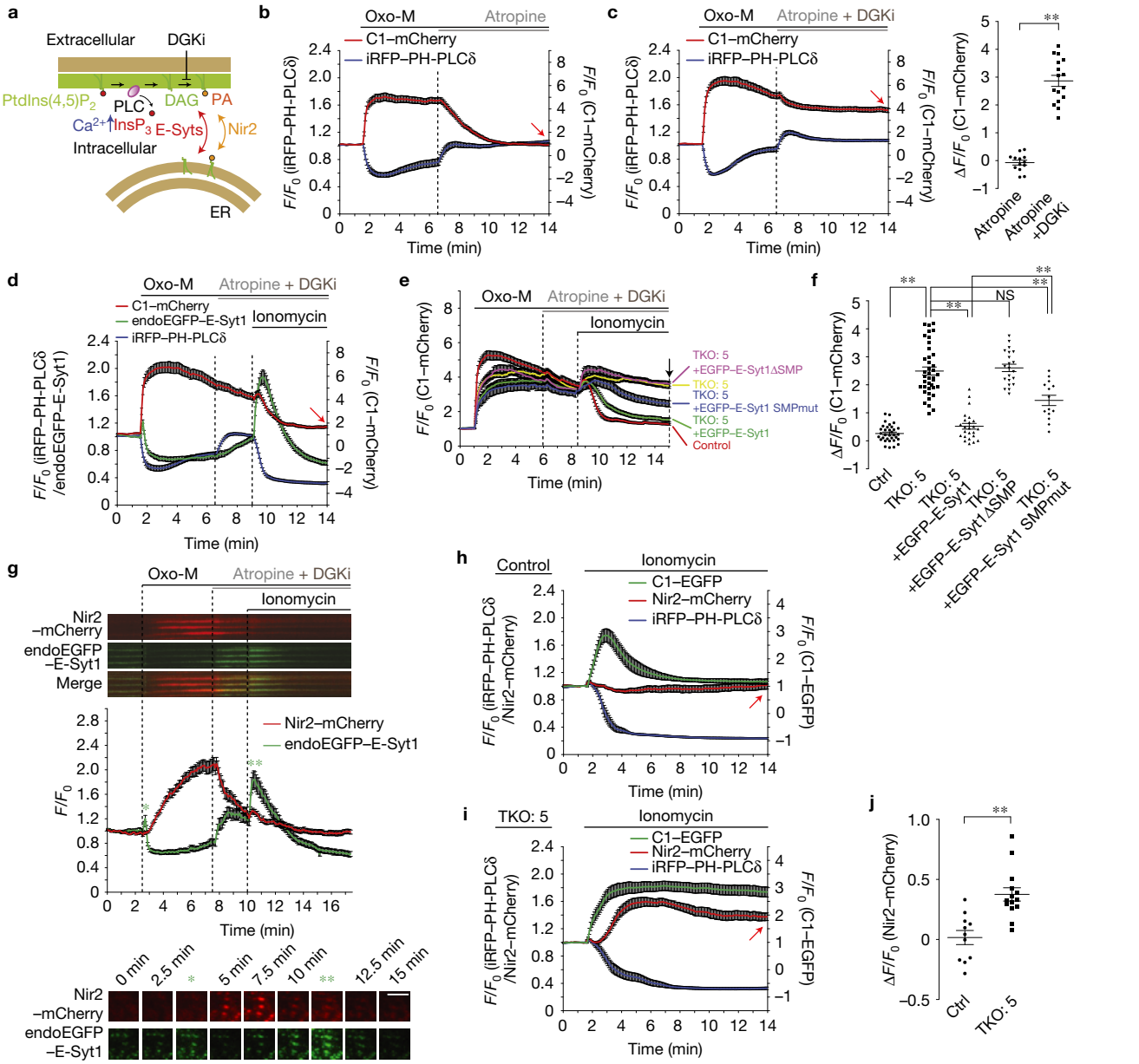

Figure 7 PM DAG extraction mediated by E-Syts. (**a**) Schematics of the possible role of E-Syts in the regulation of PM DAG dynamics during PLC activation. $InsP_3$, inositol 1,4,5-trisphosphate. (**b**,**c**) Time course of normalized fluorescence signal in response to Oxo-M (10 μM) and atropine (50 μM) (**b**) or Oxo-M (10 μM) and atropine plus DGKi (50 μM each) (**c**), as assessed by TIRF microscopy, from cells expressing M1R, iRFP–PH-PLCδ and C1–mCherry. Right, **c**: values of $\Delta F/F_0$ corresponding to the end of the experiment as shown with the red arrows in **b** and **c** (mean ± s.e.m., $n=13$ cells (Atropine), $n=16$ cells (Atropine + DGKi); two-tailed Student's *t*-test with unequal variance, $^{**}P<0.0001$). Data are pooled from two independent experiments for each condition. (**d**) Time course of normalized fluorescence signal, in response to the indicated compounds, as assessed by TIRF microscopy, from cells expressing endogenously tagged E-Syt1 co-expressing M1R, iRFP–PH-PLCδ and C1–mCherry. Compare the C1–mCherry signals indicated by the red arrow with the values in **c** (mean ± s.e.m., $n=20$ cells pooled from three independent experiments). (**e**) Time course of normalized mCherry signal, in response to the indicated compounds, as assessed by TIRF microscopy, from WT control and E-Syt TKO cells expressing C1–mCherry. (**f**) Values of F/F_0 corresponding to the end of the experiment as shown by an arrow in **e** (mean ± s.e.m., $n=33$ cells pooled from five independent experiments (Ctrl), $n=39$ cells pooled from six independent experiments (TKO:5), $n=24$ cells pooled from four independent experiments (TKO:5 + EGFP–E-Syt1), $n=21$ cells pooled from three independent experiments (TKO:5 + EGFP–E-Syt1ΔSMP), $n=14$ cells pooled from two independent experiments (TKO:5 + EGFP–E-Syt1 SMPmut); Bonferroni's multiple comparisons test, $^{**}P<0.0001$ except $P=0.0002$ for TKO:5 + EGFP–E-Syt1 versus TKO:5 + EGFP–E-Syt1 SMPmut; NS, not significant). (**g**) Time course of normalized fluorescence signal, in response to the indicated compounds as, assessed by TIRF microscopy of cells expressing endogenously tagged E-Syt1 co-expressing M1R, and Nir2 fused with mCherry (Nir2–mCherry). Mean ± s.e.m., $n=20$ Nir2-positive ER–PM contacts from two individual cells. Representative kymographs (top) and snapshots (bottom) of ER–PM contacts at different times are shown. Green asterisks indicate E-Syt1 recruitment. Scale bar, 5 μm. (**h**,**i**) Time course of normalized fluorescence signal, as assessed by TIRF microscopy, from WT control (**h**) and E-Syt TKO cells (**i**) expressing Nir2–mCherry, iRFP–PH-PLCδ and C1–EGFP. Ionomycin (2 μM) addition is indicated. (**j**) Values of $\Delta F/F_0$ corresponding to the end of the incubation as shown with red arrows in **h** and **i** (mean ± s.e.m., $n=11$ cells pooled from three independent experiments (Ctrl), $n=14$ cells pooled from four independent experiments (TKO:5); two-tailed Student's *t*-test with equal variance, $^{**}P=0.0002$).

PtdIns(4,5)P_2 recovery on atropine treatment, Nir2 dissociated from the PM whereas E-Syt1 (that is, primarily reflecting the E-Syt1/E-Syt2 heterodimer in these experiments where tagged E-Syt1 was expressed at endogenous levels) returned to its basal levels at this membrane. Furthermore, the additional very robust recruitment of E-Syt1 triggered by ionomycin did not have an effect on Nir2 (Fig. 7g and Supplementary Video 3). Nir2 and E-Syt1 recruitment occurred at the same ER–PM contact sites (see kymographs in Fig. 7g), suggesting the pre-existence of contacts that are populated by different lipid transfer proteins depending on the functional state of the cell.

Finally and importantly, robust recruitment of Nir2 to the PM was observed in cells lacking E-Syts following ionomycin treatment, but not in control cells (Fig. 7h–j), indicating a strong functional connection between the functions of the two proteins (Fig. 7h–j). As recruitment of Nir2 to the PM is thought to be dependent, at least in part, on DAG and PA presence in this membrane, these findings further support a role of the E-Syts in clearing PtdIns(4,5)P_2 lipid metabolites from the PM.

Together, these results reveal the occurrence of an E-Syt-dependent pathway for the removal of excess DAG from the PM following PLC activation, which is likely to act in cooperation with the pathway involving conversion to PA and Nir2 (refs 33,34).

DISCUSSION

Our present results provide direct evidence for the suggested ability of the E-Syts to transfer lipids between bilayers and demonstrate the impact of the E-Syts on the regulation of lipid homeostasis in the PM. They further show the importance of the Ca^{2+}-dependent regulation of E-Syt1 in its lipid transfer function.

The ability of E-Syt1 to transport lipids was proved by *in vitro* lipid transfer between liposomes mimicking the ER (no acidic phospholipids) and the PM (presence of PtdIns(4,5)P_2 and PS) respectively. In these assays, the entire cytosolic domain of E-Syt1 was anchored to the ER-like liposomes via a histidine tag, and addition of Ca^{2+} led to its interaction *in trans* with PM-like liposomes to allow lipid transfer. Transfer was bidirectional, dependent on the lipid-harbouring properties of the SMP domain and on the presence of PtdIns(4,5)P_2 in the PM-like liposomes. Moreover, transfer was driven by the concentration gradient of the lipid and strongly potentiated by the presence of Ca^{2+} in the micromolar range, consistent with recent results describing the Ca^{2+}-dependency of E-Syt1 recruitment to the PM in semi-intact cells[12]. A major role of Ca^{2+} in lipid transfer is to promote the membrane tethering function of E-Syt1, which requires the Ca^{2+}-binding properties of its C2C domain[8,11,12,37]. However, it is also possible that Ca^{2+}-dependent binding to lipid bilayers of its C2A domain, which also contains a Ca^{2+}-binding site[8,13,36], may assist lipid transfer by a direct and local effect on the bilayer. As a Ca^{2+}-sensitive C2A domain is present in E-Syt2 and E-Syt3[13], even these two proteins, whose ER to PM tethering function is not regulated by Ca^{2+}, may in fact have a Ca^{2+}-dependent role in lipid transfer. This hypothesis deserves further investigation. Collectively, *in vitro* studies demonstrate that the E-Syts facilitate passive transport of glycerolipids between bilayers along concentration gradients.

As we show here, the E-Syts are not essential for cellular life. Cells that lack expression of all three E-Syts do not exhibit major obvious defects, although they grow more slowly than controls. This lack of major defects may be explained by overlapping functions with other SMP-domain-containing proteins in mammalian cells[19]. However, yeast cells that lack all three tricalbins, which seem to be the only SMP-domain-containing homologues of E-Syts in this organism, are also viable, suggesting that the function of this protein family is not essential[10]. Accordingly, mass spectrometry analysis of PM isolated from WT and E-Syt KO cells using a one-step procedure, did not reveal a difference in the composition of the PM in the major glycerolipid species. Our study suggests that one of E-Syts' functions is to help produce adaptive changes in the PM following an acute perturbation. In cells lacking expression of all E-Syts, impaired disappearance from the cytosolic leaflet of the PM of newly generated DAG on PLC activation was observed. E-Syt1 alone could rescue the defect and rescue depended on the lipid-harbouring property of its SMP domain and required its anchorage to the ER.

Another mechanism responsible for the rapid return to basal levels of DAG after its acute generation by PLC-dependent PtdIns(4,5)P_2 cleavage is its conversion to PA in the PM, followed by PA transfer to the ER[35] at least in part via the lipid transfer protein Nir2 (and possibly also by Nir3)[34]. As the E-Syts can harbour glycerophospholipids irrespective of the headgroup, cooperation of E-Syts with Nir2 in PA transport is plausible. Like E-Syts, Nir2 is recruited to ER–PM contacts in response to PLC activation[34,37]. Our results show the recruitment of Nir2 and E-Syt1 to the PM, and thus their functions, can be decoupled. However, Nir2 and the E-Syts are functionally linked, as ionomycin stimulation induces a robust and prolonged accumulation of Nir2 at the PM in cells that lack all three E-Syts but not in control cells.

If the E-Syts can transfer promiscuously glycerolipids (and possibly other lipids), one may wonder why they do not reduce the difference in glycerolipid composition between the ER and the PM. One explanation is that their equilibrating action is continuously conteracted by mechanisms that generate diversity. Another explanation, given the Ca^{2+} dependence of their transport, is that restoring normal lipid levels in response to acute perturbations, as shown here for PM-localized DAG, may in fact be their major functions.

In summary, our study demonstrates a role for the ER-localized E-Syts in the regulation of PM lipid homeostasis via *in trans* actions at ER–PM contact sites. Our findings emphasize a role for these proteins in maintaining lipid homeostasis in response to acute perturbations. However, additional functions of these proteins are plausible. Studies in yeast and plants have pointed to increased PM fragility in cells lacking tricalbins/extended synaptotagmins[17,38–40]. The potential occurrence of other changes in the PM bilayers of E-Syt TKO cells deserves further investigation. Further elucidating the physiological roles of these proteins as well as of other SMP-domain-containing proteins localized at membrane contact sites will be important to gain insight into how non-vesicular transport of lipids between bilayers contributes to maintain the specific lipid composition of each membrane. □

METHODS

Methods and any associated references are available in the online version of the paper.

Note: Supplementary Information is available in the online version of the paper

ACKNOWLEDGEMENTS

We thank H. Shen, S. Ferguson, S. Tomita, R. Dong, W. Hancock-Cerutti, J. Lees and Y. Cai for discussion and/or sharing reagents. We thank F. Wilson, H. Czapla and L. Lucast for technical assistance. This work was supported in part by NIH grants R37NS036251, DK45735 and DA018343 to P.D.C. Y.Saheki was supported by fellowships from the Uehara Memorial Foundation and the Japan Society for the Promotion of Science, and X.B. by a Human Frontier Science Program long-term fellowship.

AUTHOR CONTRIBUTIONS

All authors participated in the design of experiments, data analysis and interpretation. Y.Saheki designed and performed all of the genetic manipulations, all of the imaging and biochemical studies and the isolation of plasma membrane sheets. X.B., F.P. and K.M.R. participated in the design of lipid transfer assays that were performed by X.B. C.M.S. and K.M.R. designed SMP domain mutations and performed lipid-binding assays. M.A.S and C.K. performed the lipidomic analysis. Y.Saheki and P.D.C. wrote the manuscript, which was then reviewed by all authors.

COMPETING FINANCIAL INTERESTS

The authors declare no competing financial interests.

Published online at http://dx.doi.org/10.1038/ncb3339
Reprints and permissions information is available online at www.nature.com/reprints

1. Holthuis, J. C. & Levine, T. P. Lipid traffic: floppy drives and a superhighway. *Nat. Rev. Mol. Cell Biol.* **6,** 209–220 (2005).
2. Elbaz, Y. & Schuldiner, M. Staying in touch: the molecular era of organelle contact sites. *Trends Biochem. Sci.* **36,** 616–623 (2011).
3. Friedman, J. R. & Voeltz, G. K. The ER in 3D: a multifunctional dynamic membrane network. *Trends Cell Biol.* **21,** 709–717 (2011).
4. Toulmay, A. & Prinz, W. A. Lipid transfer and signaling at organelle contact sites: the tip of the iceberg. *Curr. Opin. Cell Biol.* **23,** 458–463 (2011).
5. Stefan, C. J. *et al.* Osh proteins regulate phosphoinositide metabolism at ER-plasma membrane contact sites. *Cell* **144,** 389–401 (2011).
6. Mesmin, B. *et al.* A four-step cycle driven by PI(4)P hydrolysis directs sterol/PI(4)P exchange by the ER-Golgi tether OSBP. *Cell* **155,** 830–843 (2013).
7. Prinz, W. A. Bridging the gap: membrane contact sites in signaling, metabolism, and organelle dynamics. *J. Cell Biol.* **205,** 759–769 (2014).
8. Giordano, F. *et al.* PI(4,5)P2-dependent and Ca(2$^+$)-regulated ER-PM interactions mediated by the extended synaptotagmins. *Cell* **153,** 1494–1509 (2013).
9. Toulmay, A. & Prinz, W. A. A conserved membrane-binding domain targets proteins to organelle contact sites. *J. Cell Sci.* **125,** 49–58 (2012).
10. Manford, A. G., Stefan, C. J., Yuan, H. L., Macgurn, J. A. & Emr, S. D. ER-to-plasma membrane tethering proteins regulate cell signaling and ER morphology. *Dev. Cell* **23,** 1129–1140 (2012).
11. Fernandez-Busnadiego, R., Saheki, Y. & De Camilli, P. Three-dimensional architecture of extended synaptotagmin-mediated endoplasmic reticulum-plasma membrane contact sites. *Proc. Natl Acad. Sci. USA* **112,** E2004–E2013 (2015).
12. Idevall-Hagren, O., Lu, A., Xie, B. & De Camilli, P. Triggered Ca2$^+$ influx is required for extended synaptotagmin 1-induced ER-plasma membrane tethering. *EMBO J.* **34,** 2291–2305 (2015).
13. Min, S. W., Chang, W. P. & Sudhof, T. C. E-Syts, a family of membranous Ca2$^+$-sensor proteins with multiple C2 domains. *Proc. Natl Acad. Sci. USA* **104,** 3823–3828 (2007).
14. Craxton, M. Genomic analysis of synaptotagmin genes. *Genomics* **77,** 43–49 (2001).
15. Craxton, M. Evolutionary genomics of plant genes encoding N-terminal-TM-C2 domain proteins and the similar FAM62 genes and synaptotagmin genes of metazoans. *BMC Genomics* **8,** 259 (2007).
16. Levy, A., Zheng, J. Y. & Lazarowitz, S. G. Synaptotagmin SYTA forms ER-plasma membrane junctions that are recruited to plasmodesmata for plant virus movement. *Curr. Biol.* **25,** 2018–2025 (2015).
17. Perez-Sancho, J. *et al.* The Arabidopsis synaptotagmin1 is enriched in endoplasmic reticulum-plasma membrane contact sites and confers cellular resistance to mechanical stresses. *Plant Physiol.* **168,** 132–143 (2015).
18. Kopec, K. O., Alva, V. & Lupas, A. N. Homology of SMP domains to the TULIP superfamily of lipid-binding proteins provides a structural basis for lipid exchange between ER and mitochondria. *Bioinformatics* **26,** 1927–1931 (2010).
19. Kopec, K. O., Alva, V. & Lupas, A. N. Bioinformatics of the TULIP domain superfamily. *Biochem. Soc. Trans.* **39,** 1033–1038 (2011).
20. Qiu, X. *et al.* Crystal structure of cholesteryl ester transfer protein reveals a long tunnel and four bound lipid molecules. *Nat. Struct. Mol. Biol.* **14,** 106–113 (2007).
21. Oram, J. F., Wolfbauer, G., Vaughan, A. M., Tang, C. & Albers, J. J. Phospholipid transfer protein interacts with and stabilizes ATP-binding cassette transporter A1 and enhances cholesterol efflux from cells. *J. Biol. Chem.* **278,** 52379–52385 (2003).
22. Schauder, C. M. *et al.* Structure of a lipid-bound extended synaptotagmin indicates a role in lipid transfer. *Nature* **510,** 552–555 (2014).
23. Kornmann, B. *et al.* An ER-mitochondria tethering complex revealed by a synthetic biology screen. *Science* **325,** 477–481 (2009).
24. AhYoung, A. P. *et al.* Conserved SMP domains of the ERMES complex bind phospholipids and mediate tether assembly. *Proc. Natl Acad. Sci. USA* **112,** E3179–E3188 (2015).
25. Morgan, A. J. & Jacob, R. Ionomycin enhances Ca2$^+$ influx by stimulating store-regulated cation entry and not by a direct action at the plasma membrane. *Biochem. J.* **300,** 665–672 (1994).
26. Willars, G. B., Nahorski, S. R. & Challiss, R. A. Differential regulation of muscarinic acetylcholine receptor-sensitive polyphosphoinositide pools and consequences for signaling in human neuroblastoma cells. *J. Biol. Chem.* **273,** 5037–5046 (1998).
27. Horowitz, L. F. *et al.* Phospholipase C in living cells: activation, inhibition, Ca2$^+$ requirement, and regulation of M current. *J. Gen. Physiol.* **126,** 243–262 (2005).
28. Suh, B. C., Horowitz, L. F., Hirdes, W., Mackie, K. & Hille, B. Regulation of KCNQ2/KCNQ3 current by G protein cycling: the kinetics of receptor-mediated signaling by Gq. *J. Gen. Physiol.* **123,** 663–683 (2004).
29. Cohen, C. M., Kalish, D. I., Jacobson, B. S. & Branton, D. Membrane isolation on polylysine-coated beads. Plasma membrane from HeLa cells. *J. Cell Biol.* **75,** 119–134 (1977).
30. Codazzi, F., Teruel, M. N. & Meyer, T. Control of astrocyte Ca(2$^+$) oscillations and waves by oscillating translocation and activation of protein kinase C. *Curr. Biol.* **11,** 1089–1097 (2001).
31. Varnai, P. & Balla, T. Visualization of phosphoinositides that bind pleckstrin homology domains: calcium- and agonist-induced dynamic changes and relationship to myo-[3H]inositol-labeled phosphoinositide pools. *J. Cell Biol.* **143,** 501–510 (1998).
32. Gallegos, L. L., Kunkel, M. T. & Newton, A. C. Targeting protein kinase C activity reporter to discrete intracellular regions reveals spatiotemporal differences in agonist-dependent signaling. *J. Biol. Chem.* **281,** 30947–30956 (2006).
33. Merida, I., Avila-Flores, A. & Merino, E. Diacylglycerol kinases: at the hub of cell signalling. *Biochem. J.* **409,** 1–18 (2008).
34. Kim, Y. J., Guzman-Hernandez, M. L., Wisniewski, E. & Balla, T. Phosphatidylinositol-Phosphatidic Acid Exchange by Nir2 at ER-PM contact sites maintains phosphoinositide signaling competence. *Dev. Cell* **33,** 549–561 (2015).
35. Whatmore, J., Wiedemann, C., Somerharju, P., Swigart, P. & Cockcroft, S. Resynthesis of phosphatidylinositol in permeabilized neutrophils following phospholipase Cbeta activation: transport of the intermediate, phosphatidic acid, from the plasma membrane to the endoplasmic reticulum for phosphatidylinositol resynthesis is not dependent on soluble lipid carriers or vesicular transport. *Biochem. J.* **341,** 435–444 (1999).
36. Chang, C. L. *et al.* Feedback regulation of receptor-induced Ca2$^+$ signaling mediated by E-Syt1 and Nir2 at endoplasmic reticulum-plasma membrane junctions. *Cell Rep.* **5,** 813–825 (2013).
37. Chang, C. L. & Liou, J. Phosphatidylinositol 4,5-bisphosphate homeostasis regulated by Nir2 and Nir3 proteins at endoplasmic reticulum-plasma membrane junctions. *J. Biol. Chem.* **290,** 14289–14301 (2015).
38. Schapire, A. L. *et al.* Arabidopsis synaptotagmin 1 is required for the maintenance of plasma membrane integrity and cell viability. *Plant Cell* **20,** 3374–3388 (2008).
39. Yamazaki, T., Kawamura, Y., Minami, A. & Uemura, M. Calcium-dependent freezing tolerance in Arabidopsis involves membrane resealing via synaptotagmin SYT1. *Plant Cell* **20,** 3389–3404 (2008).
40. Aguilar, P. S., Engel, A. & Walter, P. The plasma membrane proteins Prm1 and Fig1 ascertain fidelity of membrane fusion during yeast mating. *Mol. Biol. Cell* **18,** 547–556 (2007).

DOI: 10.1038/ncb3339

METHODS

Antibodies and chemicals. The primary and secondary antibodies used in this study are listed in Supplementary Table 1. Oxo-M, atropine and ionomycin (Sigma-Aldrich); thapsigargin (Invitrogen/Life Technologies); DGK inhibitor (R 59-022, Tocris Bioscience); proteinase K (Sigma-Aldrich). The following concentrations of chemicals are used in all of the experiments unless noted otherwise: Oxo-M, 10 μM; atropine, 50 μM; ionomycin, 2 μM; thapsigargin, 2 μM; DGK inhibitor, 50 μM. All non-radiolabelled lipids were obtained from Avanti Polar Lipids: 1-palmitoyl-2-oleoyl-*sn*-glycero-3-phosphocholine (POPC), 850457; 1,2-dioleoyl-*sn*-glycero-3-phosphoserine (DOPS), 840035; L-α-phosphatidylinositol-4,5-bisphosphate (PtdIns(4,5)P_2), 840046; (NBD)-1,2-dipalmitoyl-*sn*-glycero-3-phosphoethanolamine (DPPE), 810144; 1,2-dioleoyl-*sn*-glycero-3-[(*N*-(5-amino-1-carboxypentyl) iminodiacetic acid) succinyl] (DGS-NTA(Ni)), 790404; 1-2-dioleoyl-*sn*-glycerol (DAG), 800811. Radiolabelled lipids were purchased from American Radiolabelled Chemicals: 1,2-dioleoyl [9,10-3H] rac-glycerol, ART 2185.

Plasmids. Untagged E-Syt1, Myc–E-Syt2 (corresponding to the previously described Myc–E-Syt2S^{78}), EGFP–E-Syt1, iRFP–PH-PLCδ1 and mRFP–PH-PLCδ1 were previously described[8,41]. The following reagents were kind gifts: mRFP–Sec61β from T. Rapoport (Harvard University, USA)[42], M1 muscarinic acetylcholine receptor (M1R) from B. Hille (University of Washington, USA)[28], ER-oxGFP from E. L. Snapp (Albert Einstein College of Medicine, USA), Nir2–mCherry from R. Dong (Yale University, USA). YFP–DBD and C1–EGFP from Addgene (plasmid no. 14874 and no. 21216)[30]. The sequences of primers used in this study are listed in Supplementary Table 2.

Cloning of EGFP–E-Syt1ΔSMP. EGFP–E-Syt1ΔSMP was generated by site-directed mutagenesis (QuickChange II-XL, Stratagene) using the primers E-Syt1_SdeI_F and E-Syt1_SdeI_R in EGFP–E-Syt1.

Cloning of EGFP–E-Syt1 V169W + L308W. Two hydrophobic amino acid residues (L308W and V169W) within the hydrophobic groove of the SMP domain were mutated to tryptophan using site-directed mutagenesis in EGFP–E-Syt1 using the primer sets E-Syt1_L308W_MF, E-Syt1_L308W_MR, E-Syt1_V169W_MF and E-Syt1_V169W_MR.

Cloning of GST–E-Syt1 SMP-C2A-C2B and GST–E-Syt1 SMP-C2A-C2B V169W+L308W. gBlock (IDT) containing E-Syt1 cDNA carrying V169W+L308W mutations was synthesized and amplified by PCR using the primer set 5′ E1_SMP_EcoRI and 3′ E1_SMP_EcoRI.

PCR products were ligated in the EcoRI site in the pDF6 vector containing E-Syt1 cDNA to generate GST–E-Syt1 SMP+C2A+C2B V169W+L308W.

Cloning of C1–mCherry. cDNA corresponding to C1 domains of C1–EGFP was excised and ligated into mCherry–N1 vector in the KpnI site. The vector was digested with BamHI and the 5′ overhang was filled by DNA Polymerase I, Large (Klenow) Fragment (NEB) to make C1 domains in-frame to mCherry.

Cell culture and transfection. HeLa cells were purchased from ATCC. They were cultured in Dulbecco's modified essential Eagle medium (DMEM; Life Technologies) supplemented with 20% (v/v) fetal bovine serum (FBS) at 37 °C and 5% CO_2. Transfection of plasmids was carried out with Lipofectamine 2000 (Life Technologies) according to the manufacturer's instructions. RNAi against endogenous E-Syt1 was carried out as described in ref. 8. Wild-type as well as genome-edited HeLa cell lines were verified as free of mycoplasma contamination by a PCR-based method. No cell lines used in this study were found in the database of commonly misidentified cell lines that is maintained by ICLAC and NCBI Biosample. All cell-based experiments were repeated at least two times.

Generation of anti-E-Syt1 antibodies. A peptide consisting of the N-terminal 19 amino acids of E-Syt1 (ERSPGEGPSPSPMDQPSAP) and an additional carboxy-terminal cysteine was synthesized by GenScript. Keyhole limpet haemocyanin (KLH) was conjugated to the cysteine residue and rabbits were immunized with the peptide. Serum was collected and polyclonal antibodies were affinity purified on the peptide used for immunization with SulfoLink Immobilization Kit for Proteins (Thermo Scientific). To further reduce nonspecific reactivity in immunofluorescence labelling of aldehyde fixed cells, the affinity-purified anti-E-Syt1 antibodies were incubated with aldehyde-fixed lysates of E-Syt1/2 DKO cells. Briefly, E-Syt1/2 DKO cells were fixed with 4% PFA in PBS at room temperature for 20 min, incubated with PBS containing 50 mM glycine at room temperature for 10 min and scraped in PBS containing 1% BSA and 0.1% Triton X-100. Affinity-purified antibodies were added to the resulting suspension and incubated at 4 °C overnight. This material was then centrifuged at 21,000*g* for 20 min at 4 °C to pellet fixed cell debris, and the supernatant was used for immunofluorescence.

Fluorescence microscopy. For imaging experiments, cells were plated on 35-mm glass-bottom dishes at low density (MatTek). Immunofluorescence and live cell imaging were carried out one day after transfection. Spinning-disc confocal (SDC) microscopy was performed using the Improvision UltraVIEW VoX system (Perkin-Elmer) built around a Nikon Ti-E inverted microscope, equipped with PlanApo objectives (40 × 1.0-NA and 60 × 1.49-NA) and controlled by Volocity (Improvision) software. Excitation light was provided by a 488-nm/50-mW diode laser (Coherent) and a 561-nm/50-mW diode laser (Cobolt), and fluorescence was detected by an EM-CCD (electron-multiplying charge-coupled device) camera (C9100-50; Hamamatsu Photonics).

Total internal reflection fluorescence (TIRF) microscopy was performed on a set-up built around a Nikon Ti-E microscope equipped with 60 × 1.49-NA. Excitation light was provided by 488-nm (for GFP), 561-nm (for mCherry/mRFP/mdsRed) and 640-nm (for iRFP) DPSS lasers coupled to the TIRF illuminator through an optical fibre. The output from the lasers was controlled by an acousto-optic tunable filter and fluorescence was detected with an EM-CCD camera (Andor iXon DU-897). Acquisition was controlled by Andor iQ software. Images were sampled at 0.20 Hz with exposure times in the 100–500 ms range. SDC microscopy was carried out at room temperature (20–25 °C) and TIRF microscopy at 37 °C.

Immunofluorescence. HeLa cells transfected with mRFP–Sec61β were washed twice with PBS and fixed with 4% PFA in PBS at room temperature for 20 min, washed with PBS and incubated with PBS containing 50 mM glycine at room temperature for 10 min. Fixed cells were permeabilized with PBS containing 1% BSA and 0.1% Triton X-100 (blocking buffer) and incubated with primary antibodies for one hour at room temperature. Cells were then washed with blocking buffer twice and incubated with Alexa Fluor 488-conjugated anti-rabbit secondary antibodies for one hour at room temperature. After 4× washing with PBS, cells were examined under a SDC microscope. Images from a mid-focal plane are shown.

Live cell imaging. Cells were washed twice and incubated with either Ca^{2+}-containing buffer (140 mM NaCl, 5 mM KCl, 1 mM $MgCl_2$, 10 mM HEPES, 10 mM glucose, and 2 mM $CaCl_2$ (pH 7.4)) or Ca^{2+}-free buffer (140 mM NaCl, 5 mM KCl, 1 mM $MgCl_2$, 10 mM HEPES, 10 mM glucose, and 3 mM EGTA (pH 7.4)) before imaging with either a SDC microscope or a TIRF microscope.

Image analysis. All fluorescent images were analysed off-line using ImageJ (NIH). Changes in PM fluorescence over time (TIRF microscopy) were analysed by manually selecting regions of interest covering the largest possible area of the cell footprint. Mean fluorescence intensity values of the selected regions were obtained and normalized to the average fluorescence intensity before stimulation after background subtraction. Quantification of fluorescence changes was performed using Excel (Microsoft) and all data are presented as mean ± s.e.m.

Electron microscopy. Cells attached to Cytodex 3 microcarrier beads (Sigma-Aldrich) were fixed in 2% glutaraldehyde–0.1 M sodium cacodylate buffer at pH 7.4. Cells were post-fixed with 1% OsO_4 in 1.5% $K_4Fe(CN)_6$–0.1 M sodium cacodylate buffer, followed by *en bloc* staining with 2% uranyl acetate in 50 mM sodium maleate buffer at pH 5.2, dehydration and embedding in Embed 812. Electron microscopy reagents were purchased from Electron Microscopy Sciences.

Biochemical analyses. *Plasma membrane isolation and protein extraction.* The procedure was modified from ref. 29. Briefly, 2*g* of Cytodex 3 microcarrier beads (Sigma-Aldrich) were reconstituted in 100 ml PBS, autoclaved and coated by incubation with a poly-D-lysine solution overnight at 37 °C. Cells were added to the reconstituted beads in sterile PETG flasks (Thermo Scientific), allowed to attach to the beads for 4 h with gentle stirring every 30 min and then further incubated overnight with continuous stirring on a rotating incubator at 37 °C with 5% CO_2. Beads were subsequently collected by spontaneous sedimentation and incubated with 220 mM sucrose, 40 mM sodium acetate, at pH 5.0 for 5 min at room temperature. This step was necessary to maximize the area of plasma membrane adherent to the beads[29]. After the acid treatment, beads were collected, incubated with a hypotonic solution (10 mM Tris-HCl, pH 8.0) and vortexed for 10 s. A 10 s sonication pulse was then applied to the beads with Virsonic 550 (Virtis) in the same solution. Beads were finally washed three times again with the same solution and either once with PBS for subsequent protein extraction with SDS lysis buffer (10 mM Tris-HCl, 150 mM NaCl, 2% SDS, pH 8.0) or with 150 mM ammonium bicarbonate for lipidomic analysis.

Lipidomics. Lipid extraction, mass spectrometric analysis and data analysis were done by Lipotype GmbH (Germany). Briefly, lipids were extracted from either total cells still attached to the beads (total lipids), or from bead-bound PMs prepared as described above (PM lipids) using chloroform and methanol[43]. Samples were spiked with lipid class-specific internal standards before extraction and lipid extracts were

immediately subjected to mass spectrometric analysis. Mass spectra were acquired on a hybrid quadrupole/Orbitrap mass spectrometer (Q-Exactive, Thermo-Fisher) equipped with an automated nano-flow electrospray ion source (Triversa Nanomate, Advion) in both positive and negative ion mode. Lipid identification using Lipotype Xplorer was performed as previously described[44].

Lipid binding to purified E-Syt1. GST-tagged E-Syt1 fragments containing the SMP domain and C2A and C2B domains (predicted molecular weight: 53.6 kDa) were generated and purified using a bacterial expression system and tested for *in vitro* lipid-binding assay as described previously[22].

Western blotting and immunoprecipitation. HeLa cells were lysed in SDS lysis buffer (10 mM Tris-HCl, 150 mM NaCl, 2% SDS, pH 8.0). Cell lysates were incubated at 60 °C for 20 min followed by incubation at 70 °C for 10 min. Benzonase nuclease (Novagen) was added, and the samples were further incubated at room temperature for 20 min. Cell lysates were loaded and separated in 8% or 4–20% SDS–PAGE gels and immunoblotting was carried out as described previously[8]. Immunoprecipitation of endogenously tagged EGFP–E-Syt1 (Fig. 1e), overexpressed EGFP–E-Syt2 (Fig. 3b) and EGFP–E-Syt1 (Supplementary Fig. 3f) was carried out using GFP-Trap beads as previously described[8].

Liposome-based experiments. *Cloning, expression and purification of an E-Syt1 fragment.* The region coding for residues 93–1104 of human E-Syt1 was cloned into the pCMV6–AN–His vector with an N-terminal His_6-tag. The protein was expressed in Expi293 cells for three days. Cells were collected and lysed by three freeze–thaw cycles (liquid N_2 and 37 °C water bath) in buffer (25 mM Tris-HCl, pH 8.0, 300 mM NaCl, 10 mM imidazole, 0.5 mM TCEP) supplemented with protease inhibitors (Complete EDTA-free; Roche). The protein was purified from the cell lysate by a Ni-NTA column (Clontech), and then further purified by gel filtration (Superdex 200, GE Healthcare) in buffer (25 mM Tris-HCl, pH 8.0, 300 mM NaCl, 0.5 mM TCEP). Fractions containing E-Syt1 were pooled and concentrated to ~1 mg ml^{-1}.

Liposome preparation. Lipids in chloroform were dried under a stream of N_2 gas followed by further drying in vacuum for 2 h. Mole percent values of lipids used for the acceptor and donor liposomes in fluorescence resonance energy transfer (FRET)-based lipid transfer experiments were as indicated in Supplementary Table 3.

The dried lipid films were hydrated with buffer (25 mM Tris-HCl, pH 8.0, 300 mM NaCl, 0.5 mM TCEP). Liposomes were then formed by ten freeze–thaw cycles (liquid N_2 and 37 °C water bath) followed by extrusion through polycarbonate filters with a pore size of 50 nm (Avanti Polar Lipids).

Dequenching (loss of self-quenching) efficiency assays. Dequenching assays of NBD were performed in 50 µl volumes containing 0.5 mM total lipids (50 µM donor liposomes containing either 1%, 3%, 5% or 7% fluorescent lipids plus 450 µM acceptor liposomes). NBD was excited at 460 nm. Self-quenching was determined by recording emission intensity at 538 nm with or without 0.5% *n*-dodecyl-ß-D-maltoside (DDM). Experiments were carried out at room temperature on a SpectraMax M5 Microplate Reader (Molecular Devices).

FRET-based lipid transfer assays. Lipid transfer reactions were performed in 50 µl volumes. The final lipid concentration in the reaction was 0.5 mM, with donor and acceptor liposomes added at a 1:9 ratio (or 1:1 for Supplementary Fig. 2e). Reactions were initiated by the addition of protein to a final concentration of 0.5 µM in a 96-well plate (Corning). The fluorescence intensity of NBD was monitored with an excitation of 460 nm and emission of 538 nm every 10 s over 30 min at room temperature by using a SpectraMax M5 Microplate Reader (Molecular Devices). All data were corrected by setting the value at the time of protein addition to zero, and subtracting the baseline values obtained in the absence of the protein. The data were expressed as a percentage of the maximum fluorescence, determined after adding 10 µl of 2.5% DDM to the reactions after 30 min.

Liposome tethering assays. Liposome tethering assays were performed as for lipid transfer assays, except that the absorbance at 405 nm was measured every 10 s over 40 min at room temperature by using a SpectraMax M5 Microplate Reader (Molecular Devices). Ten microlitres of cocktail (1.8 M imidazole, 15 mM EGTA, 1.15 mg ml^{-1} proteinase K) was added to stop the reaction after 30 min. The absorbance before protein addition was set to zero.

Content mixing assays. For content mixing assays, donor liposomes (85:15 mole percent POPC: DGS-NTA_{Ni}) and acceptor liposomes (85:10:5 mole percent POPC: DOPS: PtdIns(4,5)P_2) were formed as for lipid transfer assays, except that 50 mM sulforhodamine B (Sigma-Aldrich) was included during the hydration of donor liposomes. The donor liposomes were pelleted in a Beckman TLA-100 rotor for 10 min at 55,000 r.p.m. (20 °C) to remove unencapsulated sulforhodamine B and the pellets were resuspended in buffer (25 mM Tris-HCl, pH 8.0, 300 mM NaCl, 0.5 mM TCEP). The reactions were performed as for lipid transfer assays, except that the fluorescence intensity of sulforhodamine B was monitored with an excitation of 565 nm and emission of 585 nm.

Radiolabelled lipid transfer assays. 'Heavy' donor and 'light' acceptor liposomes were as follows. 'Heavy' liposomes: 300 µmol lipids (84:10:5:0.9:0.1 mole percent POPC: DOPS: PtdIns(4,5)P_2: DAG: tritium-labelled DAG for donor liposomes) in chloroform were dried in the vacuum for 1.5 h. The lipid films were hydrated with buffer (25 mM Tris-HCl, pH 8.0, 150 mM NaCl, 0.5 mM TCEP, 0.75M sucrose) and incubated at 37 °C for 30 min. Liposomes were then formed by five freeze–thaw cycles (liquid N_2 and 37 °C incubation), pelleted and resuspended in buffer (25 mM Tris-HCl, pH 8.0, 150 mM NaCl, 0.5 mM TCEP). 'Light liposomes' were composed of 85% POPC and 15% DGS-NTA(Ni) and were prepared as for FRET-based lipid transfer assays.

Lipid transfer reactions were performed in 100 µl volumes. The final lipid concentration in the reaction was 0.5 mM, with 'heavy' donor and 'light' acceptor liposomes added at a 1:2 ratio. Reactions were initiated by the addition of protein to a final concentration of 0.5 µM and terminated by the addition of 10 µl of a solution containing 1.8 M imidazole and 1.15 mg ml^{-1} proteinase K. 'Heavy' and 'light' liposomes were then separated by centrifugation at 16,000*g* for 15 min and 'heavy' liposomes recovered in the pellets were resuspended in 100 µl buffer (25 mM Tris-HCl, pH 8.0, 150 mM NaCl, 0.5 mM TCEP). Radioactivity present in the supernatant and in the resuspended pellets was then determined at room temperature with a Liquid Scintillation Counter 1409DSA (Wallac).

CRISPR/Cas9-mediated endogenous tagging of E-Syt1. This procedure was performed by PNAbio. Briefly, the donor vector comprising cDNA encoding EGFP with a linker sequence (SGLRSRAQASNSAVD) flanked by ~500 bp homologous recombination arms covering the 5′ end of exon1 of human E-Syt1 gene was synthesized and co-transfected in HeLa cells with the guide RNA (RG6: AATGGAGCGATCTCCAGGAGAGG) and Cas9. EGFP-positive cells were FACS enriched and individual cells were isolated. PCR-based genotyping of ~150 clones identified several candidate clones with genomic integration of the donor sequence at the endogenous E-Syt1 locus. These clones were further analysed by PCR-based genotyping, sequencing and western blotting. The endogenously tagged cells were further characterized by RNAi and microscopy as shown in the results.

Generation of E-Syt knockout HeLa cell lines. A transcription activator-like effector nuclease (TALEN) pair that targets the region encoding the SMP domain of human E-Syt2 and two CRISPR guide RNAs, E-Syt1(6) and E-Syt1(7), that target the region encoding the hydrophobic hairpin stretch of human E-Syt1 were designed (Fig. 3a). The efficiencies of the TALEN pair and CRISPR/Cas9 were estimated as 10.9%, 2.5% and 4.5% respectively using a Surveyor nuclease assay (Supplementary Fig. 3a). To enrich genome-edited cells that carry insertions or deletions (indels) at the targeted loci, the surrogate vector system[45] and fluorescence activated cell sorting (FACS) were used to enrich for cells expressing the EGFP encoded by the surrogate vector. In brief, the inserted target sequences for TALEN or Cas9 are flanked by mCherry and EGFP. Without non-homologous end joining (NHEJ)-mediated repair of DNA double-stranded breaks, the stop codon (shown in red) allows only mCherry expression. After NHEJ, frame-shift in the target sequence leads to expression of mCherry–EGFP fusion protein, resulting in an increase in EGFP signals (Supplementary Fig. 3b,c). First, KO HeLa cells for E-Syt2 were generated. The E-Syt1 and E-Syt3 genes were subsequently targeted in these cells by CRISPR/Cas9.

For the generation of HeLa cells lacking E-Syt2, WT cells were transfected with the plasmids encoding the E-Syt2-targeting TALEN pair and the surrogate vector, followed by enrichment of genome-edited cells via FACS and isolation of individual clones by dilution cloning. PCR analysis of the genomic DNA isolated from 39 individual clones verified candidate indels in the region encoding the SMP domain of E-Syt2 (Supplementary Fig. 3d). Two clones (line 10 and line 38) were further characterized with sequencing and western blotting. These analyses revealed predicted deletions within the TALEN pair-binding sites, frame-shift and early termination in the open-reading frame of the E-Syt2 gene, and the loss of E-Syt2 protein expression (Supplementary Fig. 3e,f). To generate E-Syt1/2 DKO cell lines, a subclone of E-Syt2 knockout cell line 38 (38-2) was transfected with plasmids encoding hCas9, E-Syt1 specific guide RNA expression vectors (E-Syt1 (6) or E-Syt1 (7)) and the surrogate vector, followed by FACS-mediated enrichment of fluorescent cells (see above; Supplementary Fig. 3b,c). Individually isolated clones, line 6-8 and line 7-5 (hereafter E-Syt1/2 DKO:6-8 and E-Syt1/2 DKO:7-5; in all figures and text, E-Syt1/2 DKO denotes E-Syt1/2 DKO:6-8 unless stated otherwise), showed insertion of one nucleotide within the guide RNA-targeted loci, resulting in a lack of E-Syt1 protein expression (Fig. 3b and Supplementary Fig. 3g). Immunostaining of E-Syt1/2 DKO cells with the newly generated anti-E-Syt1 antibody (see above) confirmed the absence of E-Syt1 signals in these cell lines (Supplementary Fig. 1b).

DOI: 10.1038/ncb3339

To generate E-Syt triple-knockout (TKO) cell lines, the E-Syt1/2 DKO:6-8 cell line was transfected with a plasmid encoding hCas9 and four PCR-amplified guide RNAs targeting the 5′ region of E-Syt3 (Fig. 3a). The surveyor nuclease assay showed robust cutting efficiency (∼28%), allowing isolation of knockout cells without further enrichment (Fig. 3b). Three clones that showed large indels in exon1 of E-Syt3 by sequencing were isolated and the absence of E-Syt3 protein was confirmed by IP-enrichment followed by western blotting (Fig. 3b).

Construction of TALEN, CRISPR and surrogate vectors. *TALEN for E-Syt2 knockout.* A TALEN pair targeting human E-Syt2 was assembled using the Golden-Gate ligation method as described previously[46].

Target sequence, RVDs and vector used were: TALEN-SMP_L: TGTAAAACAC ATGTGGCCTT, (NG) NN NG NI NI NI NI - HD NI HD NI NG NN - NG NN NN HD HD NG (NG), pTALEN_v2(NG);

TALEN-SMP_R: TAGTTTCTCGAAACAACTTC, (NG) NI NN NG NG NG HD - NG HD NN NI NI NI - HD NI NI HD NG NG (HD), pTALEN_v2(HD).

Surrogate vector was designed following the strategy previously published[45]. To generate a surrogate vector for the TALEN-SMP pair, the DNA oligonucleotide TALEN was synthesized and used as a template for PCR reaction.

Primers used were 5′ BglII_SMP-1 Surro and 3′ BamHI_SMP-1 Surro.

PCR products were ligated between BglII and BamHI in mCherry–E-Syt2–EGFP[8] to generate mCherry–SMP-1 Surro–EGFP.

PCR genotyping was carried out using the primer set 5′ SMP-1 N and 3′ SMP-1 Ex, which generates a 311 bp fragment in control.

TALEN-SMP_L, TALEN-SMP_R and mCherry–SMP-1 Surro–EGFP were co-transfected in HeLa cells, and EGFP-positive cells were sorted with the iCyt SY3200 (Sony) 72 h after transfection. Sorted cells were individually cloned by dilution cloning and assessed by genotyping PCR and western blotting. The sequences of oligonucleotides and primers used are listed in Supplementary Table 2.

CRISPR/Cas9 for E-Syt1 knockout and E-Syt3 knockout. E-Syt1 knockout: gBlock (IDT) comprising U6 promoter, human E-Syt1 target sequence and guide RNA was synthesized as described previously[47]. gBlock was incubated with Taq polymerase and ligated into pCR2.1 TOPO vector using the TOPO-TA cloning kit (Life Technologies); target sequences used were E-Syt1 (6) and E-Syt1 (7).

To generate a surrogate vector for the CRISPR/Ca9 targeting E-Syt1, DNA oligonucleotides E-Syt1(6,7)_F and E-Syt1(6,7)_R were synthesized, phosphorylated using T4 PNK and annealed.

Products were ligated between BglII and BamHI in mCherry–E-Syt2–EGFP[8] to generate mCherry–E-Syt1(6,7)–EGFP.

PCR genotyping was carried out using the following primer set: 5′ ESYT1_TM_F2 and 3′ ESYT1_TM_R2, which generates a 489 bp fragment in the control.

Either TOPO CRISPR E-Syt1(6) or TOPO CRISPR E-Syt1(7) together with hCas9[47] and mCherry–E-Syt1(6,7)–EGFP was co-transfected in E-Syt2 KO (line 38 described above) HeLa cells, and EGFP-positive cells were sorted with the iCyt SY3200 (Sony) 72 h after transfection. Sorted cells were individually cloned by dilution cloning and assessed by genotyping PCR and western blotting to obtain E-Syt1/2 DKO cells.

E-Syt3 knockout: gBlock (IDT) comprising U6 promoter, human E-Syt3 target sequence and guide RNA was synthesized as described previously[47]. gBlock was amplified using gRNA_F and gRNA_R primers[47]; target sequences used were P1S, P2AS, P2S and P2AS.

PCR genotyping was carried out using the primer set 5′ ESYT3_TM_F2 and 3′ ESYT3_TM_R2, which generates a 573 bp fragment in the control.

Four PCR products containing the individual guide RNA expression system together with hCas9[47] were co-transfected in E-Syt1/2 DKO (line 6-8 described in the results) HeLa cells. Cells were then individually cloned by dilution cloning 72 h after transfection and assessed by genotyping PCR to obtain E-Syt1/2/3 TKO cells.

The sequences of oligonucleotides and primers used are listed in Supplementary Table 2.

Sequencing of mutant alleles. Sequencing of mutated alleles was carried out by cloning PCR products into the pCR4 Blunt-TOPO vector using the Zero Blunt TOPO PCR cloning kit for sequencing (Life Technologies). Biallelic insertions/deletions were confirmed by sequencing at least 10 individual colonies. The same primers were used as genotyping primers.

Statistics and reproducibility. No statistical method was used to predetermine sample size. The experiments were not randomized. Comparisons of data were carried out by either two-tailed Student's *t*-tests or *t*-tests with Bonferroni correction for multiple comparisons (multiplicity adjusted *P* values are shown in the case of multiple comparisons) as appropriate with Prism 6 (GraphPad software).

Immunofluorescence experiments were repeated three times with similar results, and representative images are shown in Fig. 1a, and Supplementary Fig. 1b.

Live cell imaging experiments were repeated three times with similar results, and representative images are shown in Figs 1d,g,i, 4c,e and 7g and Supplementary Figs 1c and 3b.

Image analysis data in Figs 1h,j and 5b are from a single experiment, but representative of three independent experiments with similar results. All other assays were repeated at least two times.

Multiple electron micrographs were acquired from different beads and a representative image is shown in Fig. 4d.

For biochemical analyses when *n* was less than five experiments, individual data points are shown: Figs 2g, 4g,h and 6c and Supplementary Fig. 2a.

Western blotting and immunoprecipitation experiments shown in Fig. 1c,e were done once, and the results were confirmed by fluorescence imaging experiments shown in Fig. 1d,f, respectively. Experiments shown in Fig. 3b were repeated two times with similar results, and representative images are shown; these results were confirmed by additional experiments shown in Supplementary Figs 3e,f,g. Experiments in Supplementary Fig. 1a were repeated two times with similar results, and representative images are shown. Experiments shown in Fig. 4f were repeated three times with similar results, and representative images are shown. All of the uncropped images are shown in Supplementary Fig. 7.

41. Idevall-Hagren, O., Dickson, E. J., Hille, B., Toomre, D. K. & De Camilli, P. Optogenetic control of phosphoinositide metabolism. *Proc. Natl Acad. Sci. USA* **109,** E2316–E2323 (2012).
42. Shibata, Y. *et al.* The reticulon and DP1/Yop1p proteins form immobile oligomers in the tubular endoplasmic reticulum. *J. Biol. Chem.* **283,** 18892–18904 (2008).
43. Sampaio, J. L. *et al.* Membrane lipidome of an epithelial cell line. *Proc. Natl Acad. Sci. USA* **108,** 1903–1907 (2011).
44. Herzog, R. *et al.* A novel informatics concept for high-throughput shotgun lipidomics based on the molecular fragmentation query language. *Genome Biol.* **12,** R8 (2011).
45. Kim, H. *et al.* Surrogate reporters for enrichment of cells with nuclease-induced mutations. *Nat. Methods* **8,** 941–943 (2011).
46. Sanjana, N. E. *et al.* A transcription activator-like effector toolbox for genome engineering. *Nat. Protoc.* **7,** 171–192 (2012).
47. Mali, P. *et al.* RNA-guided human genome engineering via Cas9. *Science* **339,** 823–826 (2013).

Erratum: Control of plasma membrane lipid homeostasis by the extended synaptotagmins

Yasunori Saheki, Xin Bian, Curtis M. Schauder, Yujin Sawaki, Michal A. Surma, Christian Klose, Frederic Pincet, Karin M. Reinisch and Pietro De Camilli

Nat. Cell Biol. http://dx.doi.org/10.1038/ncb3339 (2016); published online 11 April 2016; corrected online 14 April 2016

In the version of this Article originally published online, '100 mM' in the *x* axes labels of Fig. 6c should have read '100 μM'. This has been corrected in all versions of the Article.

DOI: 10.1038/ncb3339

nature cell biology

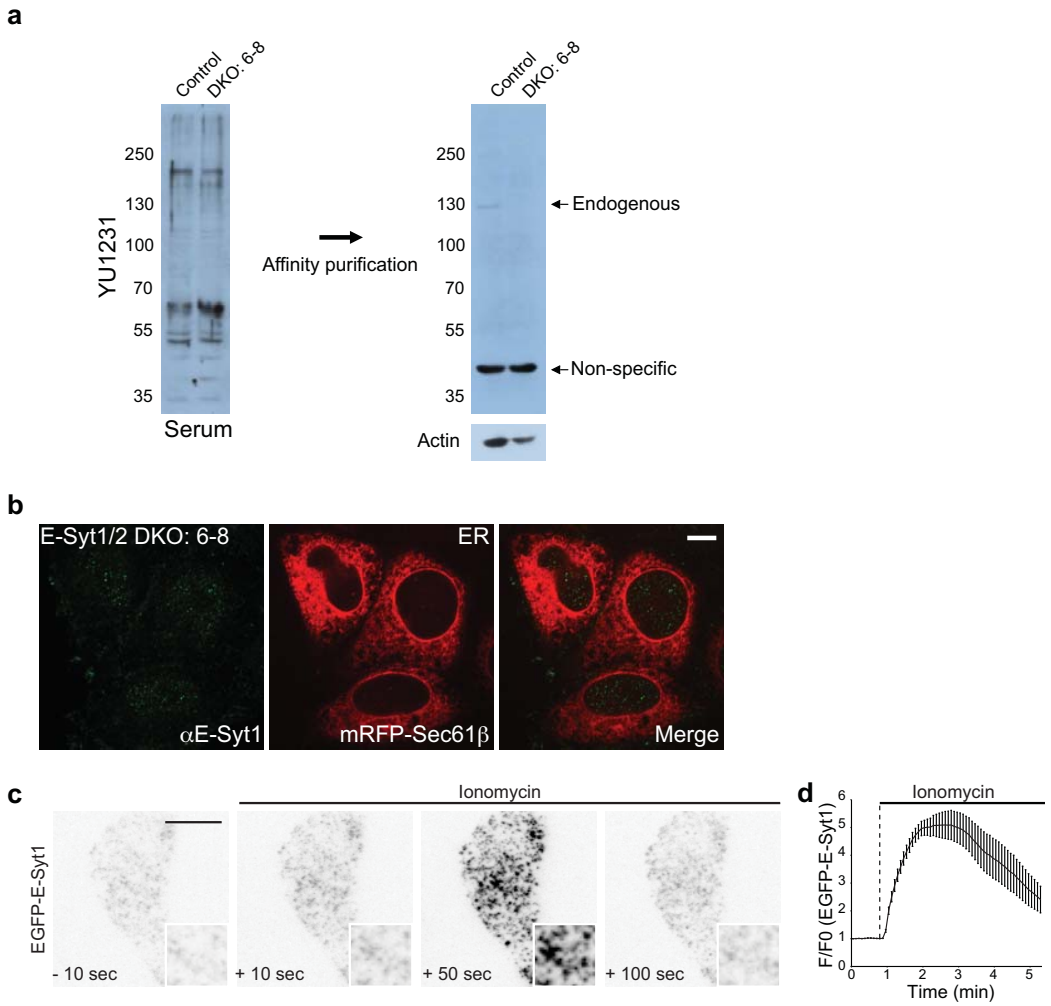

Supplementary Figure 1 Localization of E-Syt1. (a) Lysates of control and E-Syt1/2 DKO HeLa cells were processed by SDS-PAGE and immunoblotting with the original YU1231 serum (left) or affinity-purified antibodies from YU1231 serum (right). The affinity-purified antibodies were further incubated with aldehyde fixed E-Syt1/2 DKO lysates and used for immunohistochemistry. (b) Confocal images of E-Syt1/2 DKO HeLa cells expressing mRFP-Sec61β. Endogenous localization of E-Syt1 was detected by the affinity-purified antibodies after incubation with aldehyde fixed E-Syt1/2 DKO lysates (see methods). Note the absence of the E-Syt1 fluorescence signals. Scale bars, 10μm. (c) TIRF microscopy images of a HeLa cell expressing transfected EGFP-E-Syt1 before and after stimulation with ionomycin (2 μM) in the presence of extracellular Ca^{2+} at the indicated time. (d) Time-course of ionomycin-induced recruitment of EGFP-E-Syt1 to the PM, as shown in c (mean +/- SEM, n=11 cells pooled from 2 independent experiments). Scale bars, 10μm. Unprocessed original scans of blots are shown in Supplementary Fig. 7.

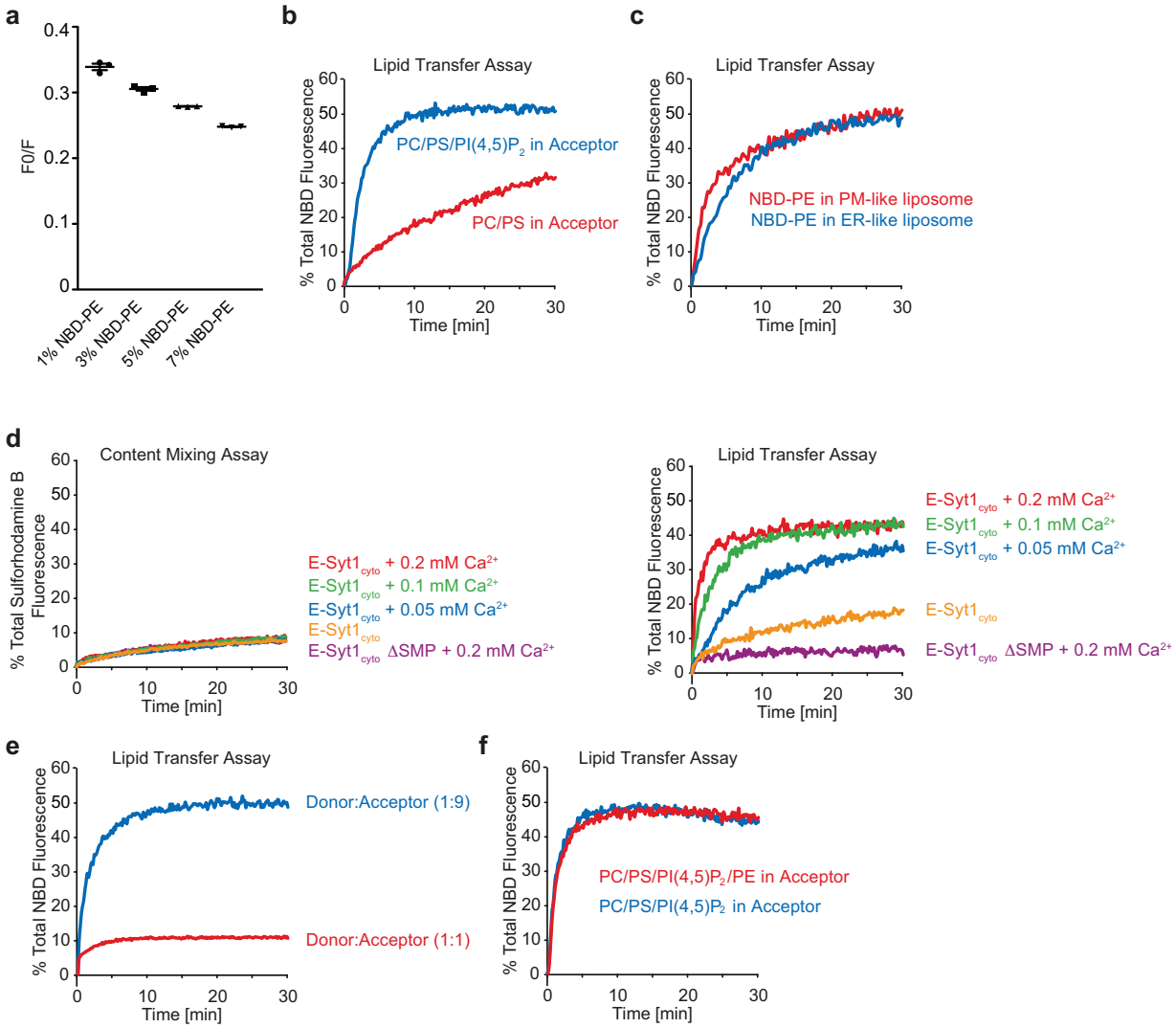

Supplementary Figure 2 Characterization of the lipid transfer assay. (a) The self-quenching property of fluorescent lipids was plotted as the ratio of the quenched fluorescence signals "FO" over the fully dequenched fluorescence signal in the presence of detergent "F" (mean +/- SEM, n=3 independent experiments) (b) Time-course of normalized fluorescence signals, as assessed by fluorometry, for the mixture of acceptor liposomes with or without $PI(4,5)P_2$ and donor liposomes containing 1% NBD-PE during an incubation with E-Syt1cyto in the presence of 100μM Ca^{2+}. Note the much slower dequenching of NBD-PE in the absence of $PI(4,5)P_2$ in the acceptor liposomes. (c) Time-course of normalized fluorescence signals, as assessed by fluorometry, for the mixture of liposomes containing 1% NBD-PE either in ER-like or in PM-like liposomes incubated with E-Syt1cyto in the presence of 100μM Ca^{2+}. Note the comparable dequenching of NBD-PE in the two conditions. (d) (left) Content mixing assay. Time-course of normalized fluorescence signals, as assessed by fluorometer, from the mixture of acceptor and donor liposomes containing self-quenched sulforhodamine B (see methods), and either E-Syt1cyto or E-Syt1cyto ΔSMP, incubated with indicated concentration of Ca^{2+} in the assay buffer. Note the minimal dequenching of sulforhodamine B that depend neither on the presence nor absence of Ca^{2+}. (right) Lipid transfer assay. Time-course of normalized fluorescence signals, as assessed by fluorometer, from the mixture of acceptor liposomes and donor liposomes containing 1% NBD-PE, and either E-Syt1cyto or E-Syt1cyto ΔSMP, incubated with indicated concentration of Ca^{2+} in the assay buffer. Note the Ca^{2+}- and SMP domain-dependent dequenching of NBD-PE fluorescence signals overtime. (e) Time-course of normalized fluorescence signal, as assessed by fluorometry, for the mixture of acceptor PM-like liposomes and donor ER-like liposomes containing 1% NBD-PE at the indicated ratios and incubated with E-Syt1cyto in the presence of 100μM Ca^{2+}. (f) Time-course of normalized fluorescence signals, as assessed by fluorometry, from the mixture of acceptor PM-like liposomes and donor ER-like liposomes. Addition of non-labeled PE to acceptor liposomes did not affect the transfer of NBD-PE. For all the liposome-based assays except a, data are from one experiment; the experiments were repeated three times with similar results.

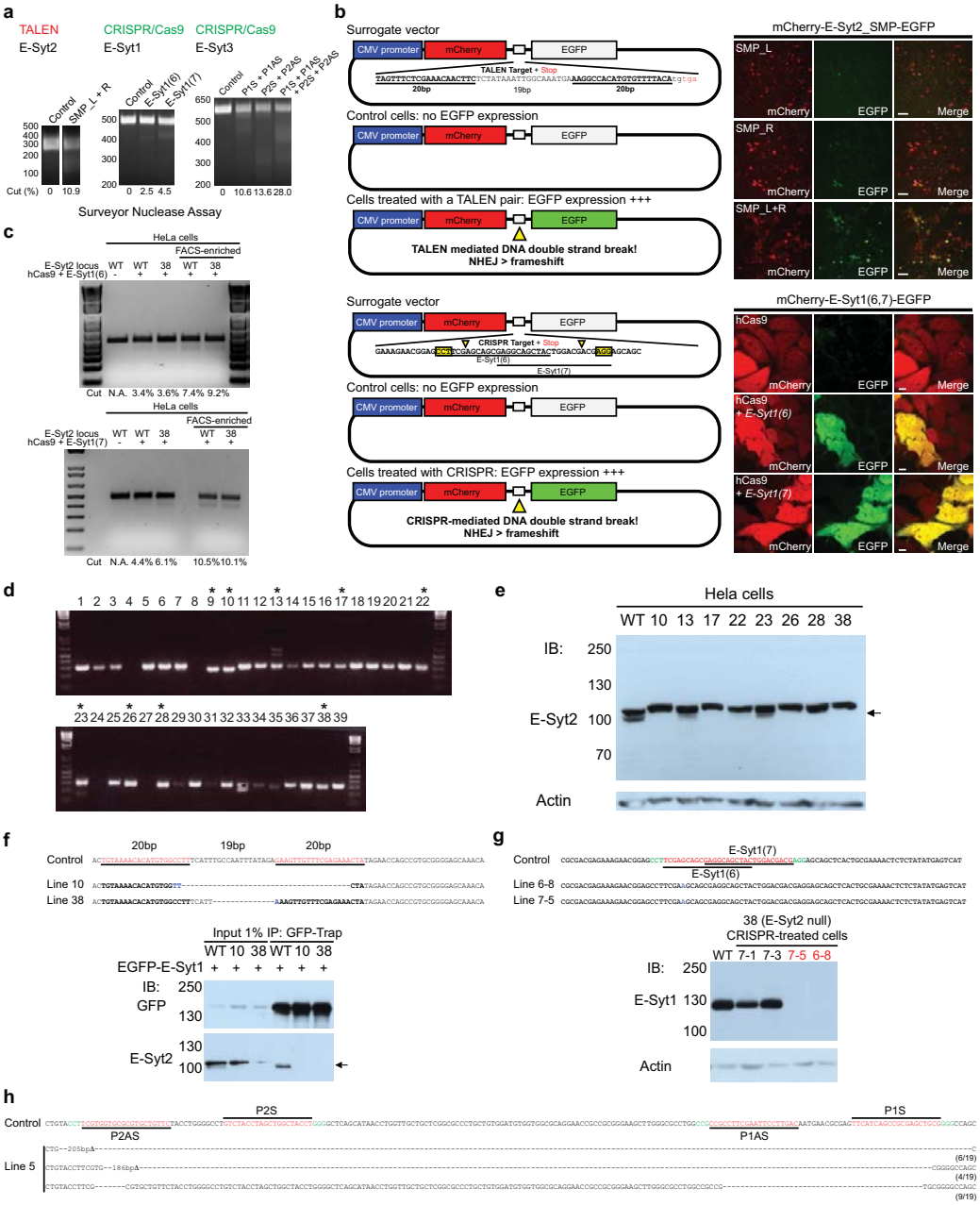

Supplementary Figure 3 Enrichment and characterization of genome-edited E-Syt knockout (KO) cells. (a) Surveyor nuclease assay for TALEN- and Cas9-mediated cleavage at E-Syt2(left), E-Syt1(middle) and E-Syt3(right) loci in HeLa cells. (b)(top left) Schematics showing the design of the surrogate vector for E-Syt2 KO. (top right) Confocal images of cells expressing the indicated TALEN constructs together with the mCherry-E-Syt2_SMP-EGFP surrogate vector. Scale bars, 100μm. (bottom left) Schematics showing the design of the surrogate vector for E-Syt1 KO. Protospacer-adjacent motif (PAM) sequences are indicated by yellow boxes; yellow allowheads indicate predicted cleavage sites. (bottom right) Confocal images of cells expressing hCas9 and the indicated guide RNA expression vectors together with the mCherry-E-Syt1(6,7)-EGFP surrogate vector. Scale bars, 10μm. (c) Surveyor nuclease assay of Cas9-mediated cleavage of E-Syt1 locus. Note approximately 2-fold increase in the cleavage efficiency after FACS. (d) Detection of TALEN-mediated cleavage of E-Syt2 gene by PCR. Asterisks denote clonal cell lines with size changes of the PCR products. (e) Lysates of control HeLa cells (WT) and 8 candidate E-Syt2 KO cell lines were processed by SDS-PAGE and immunoblotting (IB) with indicated antibodies. Arrow indicates endogenous E-Syt2. (f) (top) Nucleotide sequence analysis of the E-Syt2 gene; TALEN-binding sites are highlighted in red, and bold and blue letters indicate TALEN-binding sites and additional nucleotide insertions, respectively. (bottom) Lysates of control HeLa cells (WT) and E-Syt2 KO cell lines transfected with EGFP-E-Syt1 were processed for immunoprecipitation with anti-GFP antibodies. Total lysates (Input) as well as anti-GFP immunoprecipitates were processed by SDS-PAGE and immunoblotted with indicated antibodies. Arrow indicates endogenous E-Syt2. (g-h) KO of E-Syt1 and E-Syt3. (g,top) Sequencing analyses of the E-Syt1 gene of two E-Syt1/2 DKO cell lines show one nucleotide insertions. (g,bottom) Lysates of control HeLa cells (WT), E-Syt2 KO cell line and the same cell line treated with guide RNA expressing vectors were processed by SDS-PAGE and immunoblotted with indicated antibodies. (h) Sequencing analysis of the E-Syt3 gene of the E-Syt TKO cell line. Guide RNA-targeting sites and PAM sequences are highlighted in red and green. Unprocessed original scans of blots are shown in Supplementary Fig. 7.

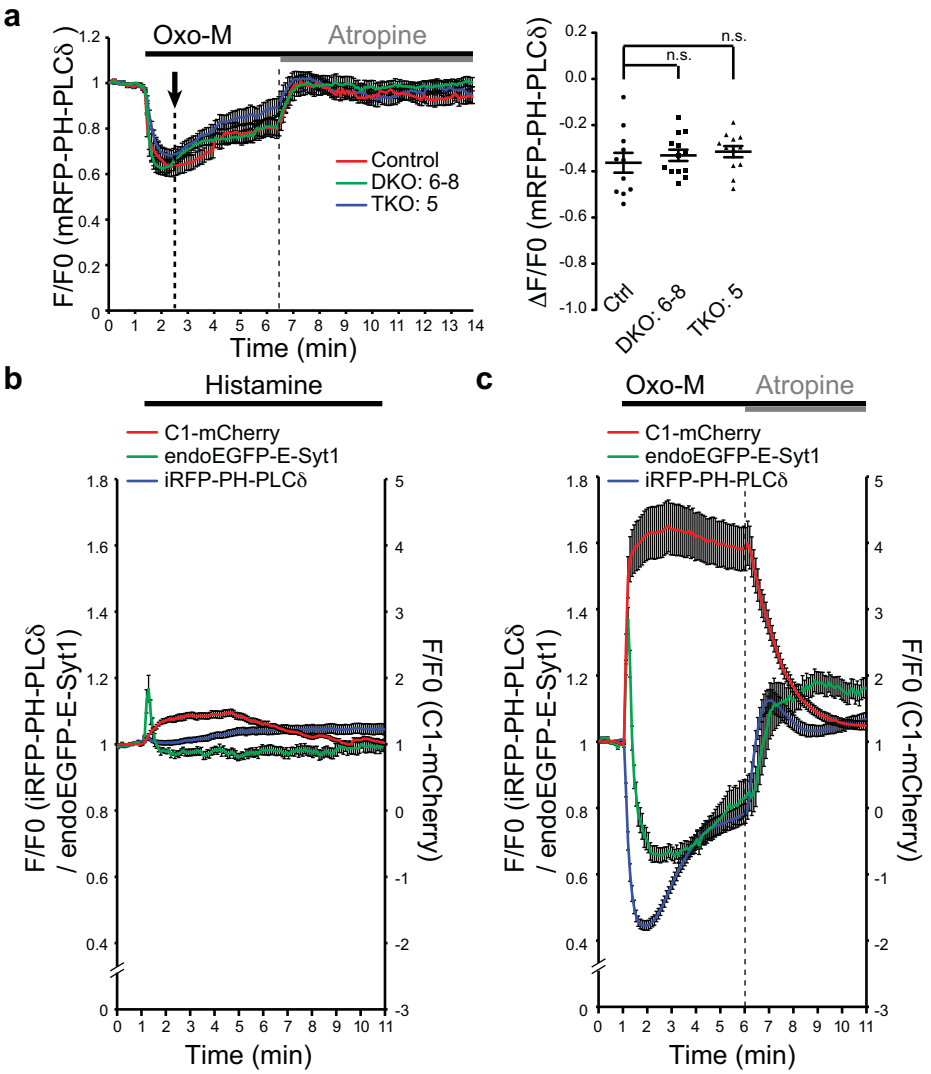

Supplementary Figure 4 PI(4,5)P_2 dynamics upon muscarinic receptor stimulation is not affected in HeLa cells lacking E-Syts. (a) (left) Time course of normalized mRFP fluorescence, as assessed by TIRF microscopy, in response to Oxo-M (10μM) and atropine (50μM), from WT control HeLa cells, E-Syt1/2 DKO HeLa cells and E-Syt TKO HeLa cells expressing mRFP-PH-PLCδ and M1R. (right) Values of ΔF/F0 corresponding to the indicated time point by arrow. [mean +/- SEM, n=11 cells (Ctrl), n=13 cells (DKO#6-8), n=12 cells (TKO#5); data are pooled from 2 independent experiments for each condition] Bonferroni's multiple comparisons test, n.s. = not significant (P>0.05). (b) Time-course of normalized EGFP, iRFP (left axis) and mCherry (right axis) fluorescence signals in response to Histamine (1mM), as assessed by TIRF microscopy, from cells expressing endogenously-tagged E-Syt1 as well as iRFP-PH-PLCδ and C1-mCherry. (mean +/- SEM, n=13 cells from 3 independent dishes) (c) Time-course of normalized EGFP, iRFP (left axis) and mCherry (right axis) fluorescence signals in response to Oxo-M (10μM) and atropine (50μM), as assessed by TIRF microscopy, from cells expressing endogenously-tagged E-Syt1 as well as M1R, iRFP-PH-PLCδ and C1-mCherry. (mean +/- SEM, n=25 cells pooled from 4 independent experiments).

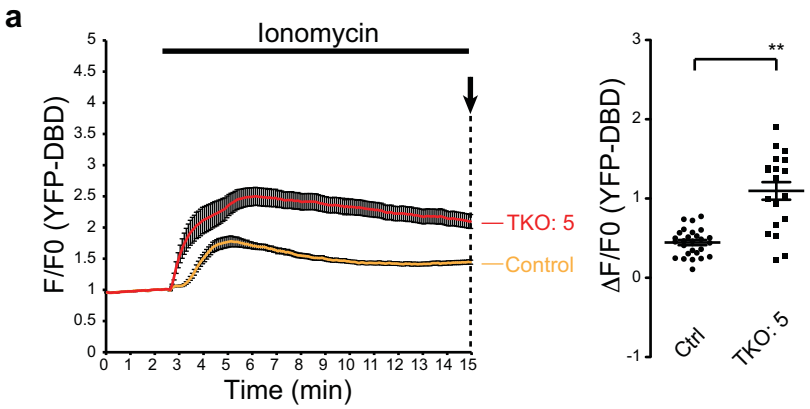

Supplementary Figure 5 Enhanced and prolonged increase of DAG in the PM of E-Syt KO cells in response to ionomycin. (a) (left) Time-course of normalized YFP fluorescence, as assessed by TIRF microscopy, from WT control and E-Syt TKO cells expressing YFP-DBD (a DAG probe), in response to ionomycin (2μM). (right) Values of ΔF/F0 corresponding to the end of the experiment as indicated by an arrow [mean +/- SEM, n=27 cells pooled from 6 independent experiments (Ctrl), n=19 cells pooled from 3 independent experiments (TKO#5); two-tailed Student's t-test with unequal variance, P<0.0001].

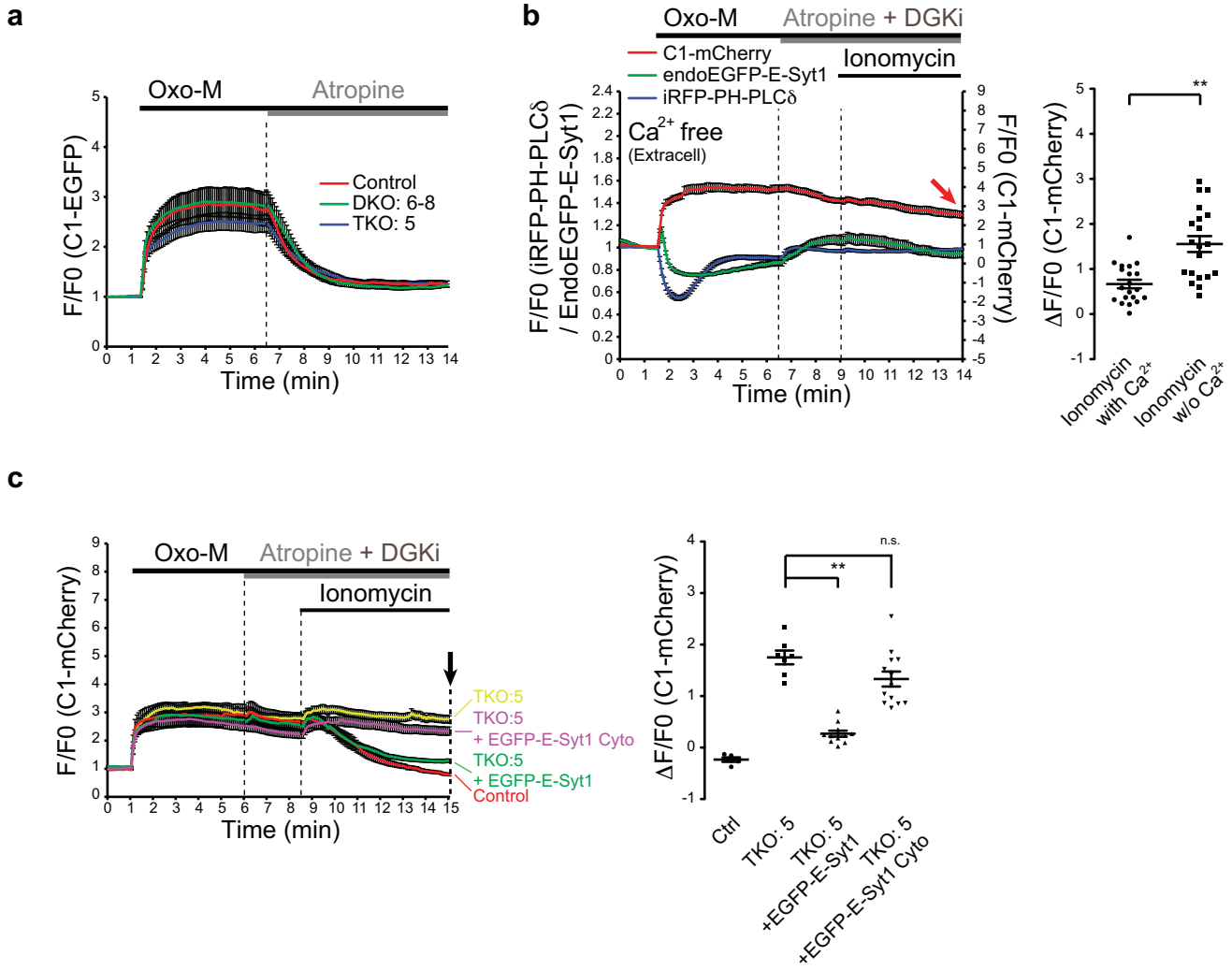

Supplementary Figure 6 Dynamics of DAG in E-Syt KO cells (a) Time course of normalized EGFP fluorescence, as assessed by TIRF microscopy, in response to Oxo-M (10μM) and atropine (50μM), from WT control HeLa cells, E-Syt1/2 DKO HeLa cells and E-Syt TKO HeLa cells expressing C1-EGFP and M1R. [mean +/- SEM, n=11 cells (Ctrl), n=13 cells (DKO#6-8), n=12 cells (TKO#5); data are pooled from 2 independent experiments for each condition] (b) (left) Time-course of normalized EGFP, iRFP (left axis) and mCherry (right axis) fluorescence signals in response to Oxo-M (10μM), atropine plus DGKi (50μM each) and ionomycin (2μM) in the absence of extracellular Ca^{2+}, as assessed by TIRF microscopy, from cells expressing endogenously-tagged E-Syt1 as well as M1R, iRFP-PH-PLCδ and C1-mCherry. (right) Values of ΔF/F0 corresponding to the end of the experiment as shown here and in Fig. 7d with red arrows [mean +/- SEM, n=20 cells (ionomycin with Ca^{2+}), n=20 cells (ionomycin without Ca^{2+}); data are pooled from 3 independent experiments for each condition; two-tailed Student's t-test with unequal variance, **denotes P=0.0001]. (c) (left) Time-course of normalized mCherry signal, in response to Oxo-M (10μM), atropine plus DGKi (50μM each) and ionomycin (2μM), as assessed by TIRF microscopy, from control (Ctrl) and E-Syt TKO cells expressing C1-mCherry. Re-expression of EGFP-E-Syt1 in E-Syt TKO cells rescued the accumulation of DAG, as assessed by C1-mCherry, while EGFP-E-Syt1 Cyto that lacks the ER anchor did not. (right) Values of F/F0 corresponding to the end of the experiment as shown with an arrow [mean+/-SEM, n=5 cells (Ctrl), n=7 cells (TKO#5), n=11 cells (TKO#5 + EGFP-E-Syt1), n=13 cells (TKO#5 + EGFP-E-Syt1 Cyto)]; data are pooled from 2 independent experiments for each condition; Bonferroni's multiple comparisons test, ** denotes P<0.0001. n.s. = not significant (P>0.05).

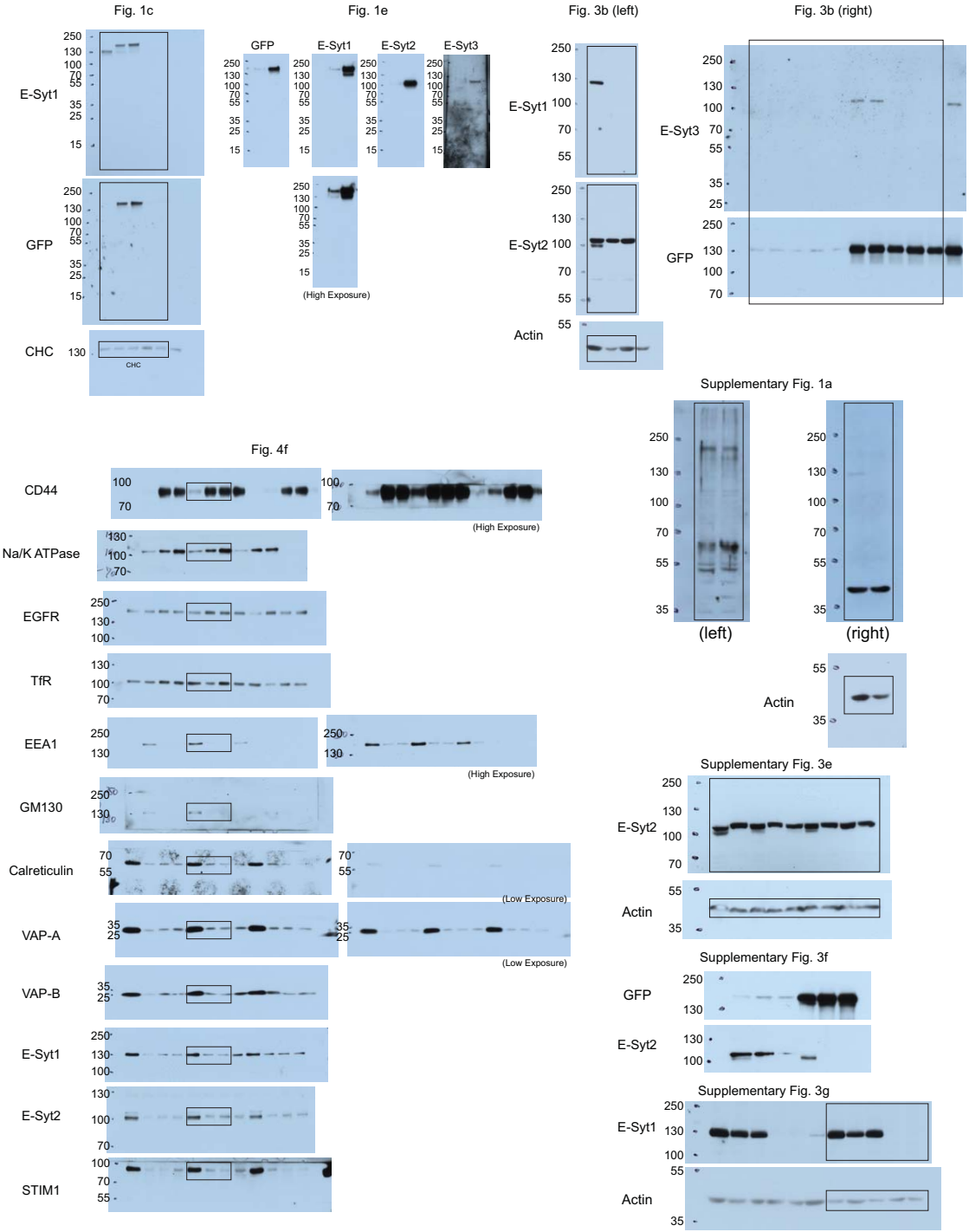

Supplementary Figure 7 Unprocessed original scans of blots used for the figures and Supplementary Figures.

Names	Catalog Numbers	Clone Numbers	Company Names	Dilution	For
anti-E-Syt1	HPA016858		Sigma-Aldrich	1/500	WB
anti-E-Syt2	HPA002132		Sigma-Aldrich	1/500	WB
anti-E-Syt3	HPA039200		Sigma-Aldrich	1/500	WB
anti-VAPA	HPA009174		Sigma-Aldrich	1/1000	WB
anti-VAPB	HPA013144		Sigma-Aldrich	1/1000	WB
anti-PDI	GTX30716	1D3	GeneTex	1/1000	WB
anti-EGFR	100-401-149		Rockland	1/1000	WB
anti-TfR	13-6800	H68.4	Invitrogen/Life-technologies	1/1000	WB
anti-actin	69100	C4	MPBiosciences	1/1000	WB
anti-STIM1	BD610954		BD	1/250	WB
anti-CD44	#5640	8E2	Cell Signaling Technology	1/1000	WB
anti-GM130	BD610822	35/GM130	BD	1/250	WB
anti-Na/K ATPase	#3010		Cell Signaling Technology	1/1000	WB
anti-EEA1	PA1-063A		Thermo Scientific	1/500	WB
anti-GFP	ab290		Abcam	1/1000	WB
anti-rabbit IgG (H+L)-HRP Conjugate	#1706515		BIO-RAD	1/5000	WB
anti-mouse IgG (H+L)-HRP Conjugate	#1706516		BIO-RAD	1/5000	WB
Alexa Fluor 488-conjugated Donkey anti-rabbit	#A21206		Invitrogen/Life-technologies	1/400	IF

WB: Western Blotting
IF: Immunofluorescence

Supplementary Table 1 Primary and secondary antibodies used in this study. Names, catalog numbers, clone numbers (only for monoclonal antibodies), company names, assays and dilution used in this study are described.

Names	Sequences
E-Syt1_SdeI_F	CTACCTGCCTGGGTCAGCTTCCCAGACGTGCCTGACCTTCAAGATGTGGCTCAGTTGCGT
E-Syt1_SdeI_R	ACGCAACTGAGCCACATCTTGAAGGTCAGGCACGTCTGGGAAGCTGACCCAGGCAGGTAG
E-Syt1_L308W_MF	TGCCTTCCTCGTGTTGCCCAACCGATGGCTGGTGCCCCTTGTGCCTGACCTTCAAGATGT
E-Syt1_ L308W _MR	ACATCTTGAAGGTCAGGCACAAGGGGCACCAGCCATCGGTTGGGCAACACGAGGAAGGCA
E-Syt1_V169W_MF	TCTGGCTGAAACTGTGGCTCCGGCTTGGAGGGGATCTAACCCCCATCTGCAAACATTTAC
E-Syt1_V169W_MR	GTAAATGTTTGCAGATGGGGGTTAGATCCCCTCCAAGCCGGAGCCACAGTTTCAGCCAGA
5' E1_SMP_EcoRI	TGGGATCCGAATTCGAGCTCGGCGCGGACGTGGAAAAGGC
3' E1_SMP_EcoRI	CAGCAGGTGAATTCGAATAATGCCCCTGGGCAGAGGGGAAC
TALEN	TGTAAAACACATGTGGCCTTTCATTTGCCAATTTATAGAGAAGTTGTTTCGAGAAACTA
5' BglII_SMP-1 Surro	CCGGACTCAGATCTTTTAGTTTCTCGAAACAACTTCTC
3' BamHI_SMP-1 Surro	CGACCGGTGGATCCTCACATGTAAAACACATGTGGCCTTTC
5' SMP-1 N	ACAACAAGATCCTCCCGCCCTTT
3' SMP-1 Ex	CAGCAATCTGACTGTGTGCAC
E-Syt1 (6)	GTAGCTGCCTCGCTGCTCGA
E-Syt1 (7)	GAGGCAGCTACTGGACGACG
E-Syt1(6,7)_F	GAGCTGTACAAGAGATCTTTGAAAGAACGGAGCCTTCGAGCAGCGAGGCAGCTACTGGAC
E-Syt1(6,7)_R	GTGGCGACCGGTGGATCCGCTGCTCCTCGTCGTCCAGTAGCTGCCTCGCTGCTCGAAGGC
5' ESYT1_TM_F2	ATCGCAAGACTAGGCAACCTCCAGCCAGTC
3' ESYT1_TM_R2	CTATGCTGCACAGAGGACCGAGGGTGGTCG
P1S	TTCATCAGCCGCGAGCTGCGGGG
P2AS	GTCAAGGAATTCGAAGGCGGCGG
P2S	GTCTACCTAGCTGGCTACCTGGG
P2AS	GAACAGCACGCGCACCACGAAGG
5' ESYT3_TM_F2	CATTTCCAGGCGCTGCTCTCCGTCGCAGAG
3' ESYT3_TM_R2	CGCAAGTTCCTCCGAACCTCGAAAGGCATC

Supplementary Table 2 Sequences of primers and oligos used in this study. Names and DNA sequences of primers and oligos as well as TALEN and CRISPR target sequences used in this study are described.

For all experiments except for those shown in Supplementary Fig. 2b, 2c and 2f.

Donor liposomes: 84% of 1-palmitoyl-2-oleoyl-sn-glycero-3-phosphocholine (POPC); 1% of 7-nitrobenzoxadiazole (NBD)-1,2-dipalmitoyl-sn-glycero-3-phosphoethanolamine (DPPE); 15% of 1,2-dioleoyl-*sn*-glycero-3-[(N-(5-amino-1-carboxypentyl) iminodiacetic acid) succinyl] (DGS-NTA_{Ni}).
Acceptor liposomes: 85% of 1-palmitoyl-2-oleoyl-sn-glycero-3-phosphocholine (POPC); 10% of 1,2-dioleoyl-sn-glycero-3-phosphoserine (DOPS); 5% of L-α-phosphatidylinositol-4,5-bisphosphate ($PI(4,5)P_2$)

For experiments of Supplementary Fig. 2b (PC/PS in Acceptor):

Donor liposomes: 84% of 1-palmitoyl-2-oleoyl-sn-glycero-3-phosphocholine (POPC); 1% of 7-nitrobenzoxadiazole (NBD)-1,2-dipalmitoyl-sn-glycero-3-phosphoethanolamine (DPPE); 15% of 1,2-dioleoyl-*sn*-glycero-3-[(N-(5-amino-1-carboxypentyl) iminodiacetic acid) succinyl] (DGS-NTA_{Ni})
Acceptor liposomes: 85% of 1-palmitoyl-2-oleoyl-sn-glycero-3-phosphocholine (POPC); 15% of 1,2-dioleoyl-sn-glycero-3-phosphoserine (DOPS)

For experiments of Supplementary Fig. 2c, the following liposomes pairs were used:

NBD-PE in PM-like liposomes:

Donor liposomes: 84% of 1-palmitoyl-2-oleoyl-sn-glycero-3-phosphocholine (POPC); 10% of 1,2-dioleoyl-sn-glycero-3-phosphoserine (DOPS); 5% of L-α-phosphatidylinositol-4,5-bisphosphate ($PI(4,5)P_2$); 1% (NBD)-1,2-dipalmitoyl-sn-glycero-3-phosphoethanolamine (DPPE)
Acceptor liposomes: 85% of 1-palmitoyl-2-oleoyl-sn-glycero-3-phosphocholine (POPC); 15% of 1,2-dioleoyl-*sn*-glycero-3-[(N-(5-amino-1-carboxypentyl) iminodiacetic acid) succinyl] (DGS-NTA_{Ni})

NBD-PE in ER-like liposomes:

Donor liposomes: 84% of 1-palmitoyl-2-oleoyl-sn-glycero-3-phosphocholine (POPC); 1% of 7-nitrobenzoxadiazole (NBD)-1,2-dipalmitoyl-sn-glycero-3-phosphoethanolamine (DPPE); 15% of 1,2-dioleoyl-*sn*-glycero-3-[(N-(5-amino-1-carboxypentyl) iminodiacetic acid) succinyl] (DGS-NTA_{Ni}).
Acceptor liposomes: 85% of 1-palmitoyl-2-oleoyl-sn-glycero-3-phosphocholine (POPC); 10% of 1,2-dioleoyl-sn-glycero-3-phosphoserine (DOPS); 5% of L-α-phosphatidylinositol-4,5-bisphosphate ($PI(4,5)P_2$)

For experiments of Supplementary Fig. 2f (PC/PS/$PI(4,5)P_2$/PE in Acceptor):

Donor liposomes: 84% of 1-palmitoyl-2-oleoyl-sn-glycero-3-phosphocholine (POPC); 1% of 7-nitrobenzoxadiazole (NBD)-1,2-dipalmitoyl-sn-glycero-3-phosphoethanolamine (DPPE); 15% of 1,2-dioleoyl-*sn*-glycero-3-[(N-(5-amino-1-carboxypentyl) iminodiacetic acid) succinyl] (DGS-NTA_{Ni}).
Acceptor liposomes: 84% of 1-palmitoyl-2-oleoyl-sn-glycero-3-phosphocholine (POPC); 10% of 1,2-dioleoyl-sn-glycero-3-phosphoserine (DOPS), 5% of L-α-phosphatidylinositol-4,5-bisphosphate ($PI(4,5)P_2$); 1% 1,2-dipalmitoyl-sn-glycero-3-phosphoethanolamine (DPPE)

Supplementary Table 3 Moles percent of lipids used for the acceptor and donor liposomes in FRET-based lipid transfer experiments.

Supplementary Video Legends

Supplementary Video 1 Rapid translocation of endogenously tagged E-Syt1 to the cortical regions of a cell, as monitored by spinning disc confocal microscopy, in response to stimulation with ionomycin (2μM).

Supplementary Video 2 Rapid translocation of endogenously tagged E-Syt1 to the cortical regions of a cell, as monitored by spinning disc confocal microscopy, in response to thapsigargin (2μM).

Supplementary Video 3 Simultaneous TIRF imaging of Nir2-mCherry and endogenously-tagged E-Syt1 (endoEGFP-E-Syt1) in response to the sequential application of Oxo-M (10μM), atropine plus DGKi (50μM each) (ATR&DGKi) and ionomycin (2μM) (Ion.) as indicated. The increase of fluorescence in the TIRF field is both diffuse and spotted for Nir2 (as this protein is both soluble and partially anchored in the ER via its interaction with VAP [36]), while it is only spotted for E-Syt1, which is an intrinsic protein of the ER. Dark spots represent ER-PM contacts.